On optimizing the aerodynamic load acting on the turbine shaft of PMSG-based direct-drive wind energy conversion system

Chen, Jiawei; Chen, Jie; Gong, Chunying

2013

Chen, J., Chen, J., & Gong, C. (2014). On Optimizing the Aerodynamic Load Acting on the Turbine Shaft of PMSG-Based Direct-Drive Wind Energy Conversion System. IEEE Transactions on Industrial Electronics, 61(8), 4022-4031.

https://hdl.handle.net/10356/96660

https://doi.org/10.1109/TIE.2013.2284148

On Optimizing the Aerodynamic Load Acting On the Turbine Shaft of PMSG-Based Direct-Drive Wind Energy Conversion System

Journal:	*Transactions on Industrial Electronics*
Manuscript ID:	13-TIE-1170
Manuscript Type:	Regular paper
Manuscript Subject:	Renewable Energy Systems
Keywords:	Wind power generation, Permanent magnet generators, Wind energy
Are any of authors IEEE Member?:	Yes
Are any of authors IES Member?:	Yes

On Optimizing the Aerodynamic Load Acting On the Turbine Shaft of PMSG-Based Direct-Drive Wind Energy Conversion System

***Abstract*—The blade's rotational sampling to the spatial distributed wind velocities will induce 3P oscillating aerodynamic torque during the wind energy generation process. This causes the turbine drive-train bare high aerodynamic load because the generator is driven by this aerodynamic torque through it. Moreover, the system inherent resonant mode will also be induced by the aerodynamic load, causing fatal damage to the whole system. To damp the serious aerodynamic load of the PMSG-based direct-drive wind energy conversation system (WECS), a new power control strategy with damping injection is proposed in this paper. The proposed method is realized by adding a compensation torque, which is proportional to the small-signal value of the generator speed, into the system torque control loop. Both the aerodynamic load and the system inherent resonant mode can be well damped if the proposed method had been adopted. Theoretic analysis is verified by experimental results performed by a 10kW WECS established in the laboratory.**

***Index Terms*—wind power generation; PMSG; aerodynamic load; natural resonant mode suppression; damping injection; power spectrum density**

NOMENCLATURE

v, V_N	Wind velocity and rated wind velocity (m/s)
C_p, C_{pmax}	Power coefficient and its maximum value
C_T, C_{Tmax}	Torque coefficient and its maximum value
λ, λ_{opt}	Tip speed ratio and its optimum value
k_T	Fit coefficient
J_r	Moment of inertia of the blade (kg·m^2)
J_g	Moment of inertia of the generator (kg·m^2)
K_s	Shaft stiffness (kg/s^2)
B_s	Friction coefficient (kgm/s)
R	Radius of the turbine (m)
ρ	Air density (kg/m^3)
ω_r, ω_g	Rotor speed and generator speed (rad/s)
ω_{ref}	Generator speed reference signal (rad/s)
ω_{rN}, ω_{gN}	Rated rotor and generator speed (rad/s)
θ_s	Shaft electrical angle (rad)
T_r, T_g	Aerodynamic and generator torque (N·m)
T_s	Shaft torque (N·m)
$T_{g,comp}$	Compensation torque (N·m)
k_g	Torque amplification gain
V_{dc}, V_l	DC-link and DC-bus voltage (V)
i_{dc}	DC-link current (A)
ω_n	Natural resonant frequency (rad/s)
ξ	System inherent damping factor (kgm/s)
K_{comp}	Compensation gain
P_r	Aerodynamic power (W)
P_{dc}	Generated power of the WECS (W)
P_{rN}, P_{dcN}	Rated aerodynamic and electrical power (W)

I. INTRODUCTION

The development in the use of renewable energy is becoming the key solution to the serious energy crisis and environment pollution now. Among various kinds of renewable energy, wind energy is by far the fastest growing energy for its free availability, environmental friendliness, policies fostering, and the maturity of turbine techniques; and, it has become a research focus and priority all over the world [1]-[3].

Nowadays, the most commonly used variable-speed turbine structures are doubly fed induction generator (DFIG) based wind energy conversion system (WECS) and direct-drive permanent-magnet synchronous generator (PMSG) based WECS [4]-[5]. To the DFIG, the presence of a gearbox that couples the wind turbine to the generator causes problems. The gearbox suffers from faults and requires regular maintenance. The reliability of the variable-speed wind turbines can be improved significantly by using the PMSG, because of which it has received much attention in wind energy application now. In addition, the PMSG based WECS also has the property of simple structure, high power factor and high efficiency. Therefore, the system structure under consideration in this paper is chosen as the direct-drive PMSG-based WECS.

The main components of a direct-drive PMSG based WECS include a turbine rotor, a drive-train, a PMSG, a full rated power electronic conversion system, and a transformer for grid connection. The system energy generation process can be typically synthesized as: the wind turbine captures the power from wind by means of turbine blades and convert it to mechanical power. The PMSG is driven by the rotating turbine through the drive-train and convert the energy from mechanical to electrical. After adjusting by the power electronics system, the generated power is then injected into the utility grid [6]-[7]. During this process, because the wind speed distribution is far from being uniform throughout the area swept by the blades of a wind turbine (the swept area is very large), wind speeds measured at different points of the swept area may substantially differ, both in its mean and turbulent components, known as wind shear effect [6]. In addition, to a horizontal wind turbine, the airflow in front of the tower is forced to bypass it, making the airflow take a lateral speed whereas its axial speed decreases, called tower shadow effect [6]. The wind shear and tower shadow effects will induce 3nP (n=1, 2, 3…) (mainly 3P) oscillating component in the captured aerodynamic torque and

further make the drive-train bear high torque ripple, defined as aerodynamic load in this paper, because the 3P oscillating torque is propagating down the system through it. The direct impacts brought by the aerodynamic load are: on the one hand, the drive-train is more likely to be fatigue breakdown, thus to shorten the useful life of the WECS; on the other hand, the system inherent resonant mode will be easily excited because the drive-train shaft of the multi-pole PMSG-based WECS is rather "soft" and prone to oscillation according to references [8]. This oscillation will leads to the fluctuation in the output power with a frequency usually being as low as 0.1–10Hz which tends to coincide with the frequencies associated with power system interarea oscillations (0.1–2.5 Hz) [9]. As a result, instability issues are expected for the power system with high wind-power penetrations if no aerodynamic load mitigation technique is adopted for the PMSG-based WECS.

In order to damp the aerodynamic load, suppress the oscillations and avoid instability, the most commonly used method is to add external damping to the WECS. A popular way is to mount the damping rubber on the drive-train shaft. However, it is costly and needs additional installation space on the drive-train shaft. Another choice, which can be seen in [10], is to apply damping by means of blade pitching for variable pitch WECS. However, this scheme requires a fast regulation of the blade pitches. The most useful way is to apply active-damping techniques either on the generator-side or on the grid-side [11]–[15]. Consider the fact that the grid-side inverter is usually used to adjust the active and reactive power of the WECS to meet the grid code, there is no more control flexible to achieve damping injection [12]-[14]. Therefore, active damping from the generator-side becomes a better choice and some researches can be found in the published literatures. In [8], [15], a damping strategy is proposed to control the stator current and the energy stored in the dc-link capacitor. By periodically short-term charging and discharging the dc-link capacitor, energy is stored in the capacitor and the load current varies. This in turn influences the torque in such a way that it counteracts the oscillations and provides effective damping. However, accurate identification of the frequency and phase angle of the generator speed oscillations is needed.

The intended contribution of this paper is to demonstrate that the difficulty to damp the aerodynamic load and suppress the oscillations can be achieved by a power control strategy with damping injection proposed. The rest of this paper is organized as follows: the PMSG-based direct-drive WECS under consideration is modeled as a two-mass model in section II, where the system inherent damping and natural resonant frequency is obtained through modeling analyses. In section III, a novel active-damping injection scheme is proposed to mitigate the aerodynamic load. Since the proposed scheme requires the knowledge of the small signal value of the generator speed, an estimation method based on the power flow analysis is further proposed to obtain this signal. Before conclusions, a fourth part gives out the experimental verifications performed by a 10kW PMSG-based direct-drive variable-speed WECS.

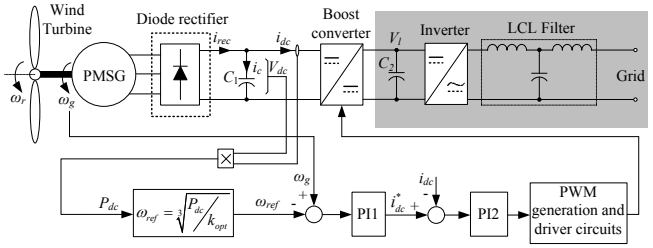

Fig.1 System configuration of the adopted 10kW PMSG-based direct-drive variable-speed WECS

II. System Modeling and Analysis

A. System Structure

The system configuration studied in this paper is depicted in Fig.1. It is constructed by a PMSG-based direct-drive fixed-pitch wind turbine. Through a diode rectifier, the output power of PMSG is transferred to a boost converter which is used to optimally regulate the output power of the turbine. The optimized power is then connected to the grid by the inverter. To balance the generated power and the power injected into the grid, the dc-bus voltage V_l is usually controlled stable by the inverter [16]-[17]. Hence, it is reasonable to treat the dc-bus voltage as an ideal voltage source when analyzing the power control strategy of the turbine. Meanwhile, the power optimization is achieved by introducing the well known power feedback control method into the control system, as shown in the lower part of Fig.1 [18]-[19]. In this method, the output power of the turbine P_{dc} is firstly sensed and used to calculate the optimum generator speed reference according to the pre-learned aerodynamic characteristics. If the generator speed is controlled to follow this optimum reference very well, the output power can be easily optimized. In addition, to make the electrical torque controllable in the adopted system structure, torque control loop is further adopted which is indirectly realized by controlling the dc-link current i_{dc}, as dipicted in Fig.1.

B. System Modeling

The well known modeling method for the WECS is using subsystem modeling method. This method first separates the whole system into several interconnected subsystems and then modeling each subsystem so as to obtain the entire system model. The system shown in Fig.1 can be structured as aerodynamic subsystem, mechanical subsystem and electrical subsystem. The modeling methods for each subsystem are given in the following.

1). *aerodynamic subsystem*

According to the Aerodynamics, the aerodynamic power and torque captured by the turbine blades can be expressed as

$$P_r = \frac{1}{2}\rho\pi R^2 \cdot C_p(\lambda) \cdot v^3 \tag{1}$$

$$T_r = \frac{1}{2}\rho\pi R^3 \cdot C_T(\lambda) \cdot v^2 \tag{2}$$

Since the fixed-pitch wind turbine is adopted in this paper, its power coefficient $C_p(\lambda)$ and torque coefficient $C_T(\lambda)$ (as shown in Fig.2 (a) and (b) respectively) are only varied with

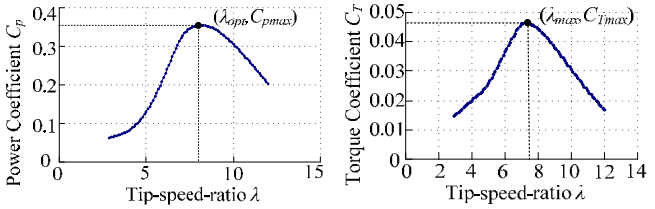

(a) (b)

Fig.2 Power and torque coefficient of the adopted turbine: (a) power coefficient; (b) torque coefficient.

tip-speed-ratio λ and they satisfy

$$C_p(\lambda) = \lambda C_T(\lambda) \tag{3}$$

where in (1)-(3), the tip-speed-ratio λ is a parameter defined as

$$\lambda = \frac{\omega_r R}{v} \tag{4}$$

Using polynomial approximation to the C_T-λ curve, we have

$$C_T(\lambda) = C_{T\max} - k_T(\lambda - \lambda_{\max})^2 \tag{5}$$

To the adopted wind turbine, $C_{T\max}$=0.048, $\lambda_{\max}$=7.2, k_T=0.002254. Detailed parameters of the WECS are shown in Table I.

2). *mechanical subsystem*

Conceptually, the mechanical structure can be arranged into several rigid bodies linked by flexible joints. The amount of these joints or degrees of freedom determines the order of the model. Even a few degrees of freedom will give rise to high order nonlinear models. Therefore, it is important to consider in the model just those degrees of freedom that are directly coupled to the control. According to [20], although simple models may not characterize thoroughly the dynamic behavior of the entire WECS, much can be learnt from them. Particularly, simple models are very helpful for analysis on power control strategies and for the controller design, whereas the unmodeled dynamics can be treated as uncertainties. By this reason, the model presented here includes just the torsion mode of the drive-train, as shown in Fig.3, where the drive-train is modeled as two rigid bodies linked by a flexible shaft. Thus, from Fig.3, one can obtain the model of the mechanical subsystem as

$$\begin{bmatrix} \dot{\theta}_s \\ \dot{\omega}_r \\ \dot{\omega}_g \end{bmatrix} = \begin{bmatrix} 0 & 1 & -1 \\ -K_s/J_r & -B_s/J_r & B_s/J_r \\ K_s/J_g & B_s/J_g & -B_s/J_g \end{bmatrix} \cdot \begin{bmatrix} \theta_s \\ \omega_r \\ \omega_g \end{bmatrix} + \begin{bmatrix} 0 & 0 \\ 1/J_r & 0 \\ 0 & -1/J_g \end{bmatrix} \cdot \begin{bmatrix} 0 \\ T_r \\ T_g \end{bmatrix} \tag{6}$$

3). *electrical subsystem*

To the WECS, consider the fact that the mechanical time constant is much greater than the electrical time constant because of the system high moment of inertia. Therefore, it is reasonable to assume the generator torque to track the torque reference without delay. Based on this assumption, we have

$$T_g = k_g T_g^* \tag{7}$$

Normally, the torque dynamic is much faster than the speed dynamic for a generator because of its large inertia. That is equally saying, the dc-link voltage (i.e. the generator

TABLE I PARAMETERS OF WECS

Parameters of the turbine	Value	Parameters of the PMSG	Value
Radius of the turbine R (m)	3.7	Shaft stiffness K_s (N·m/rad)	620
Numbers of blades	3	Friction Coefficient B_s (N·m·s/rad)	0.14
Moment of inertia of the blade J_r (kg·m^2)	38	Moment of inertia of the generator J_g (kg·m^2)	0.32
Rated rotor power P_{rN} (kW)	10	Rated output power P_{dcN} (kW)	10
rated wind velocity V_N (m/s)	10.5	Permanent Magnet Flux ψ (wb)	1.28
Max power coefficient C_{pmax}	0.35	Rated rotor speed ω_N (RPM)	500
Optimum tip-speed-ratio λ_{opt}	8.2	Winding Resistance R_s (Ω)	3.6
Rated rotor speed ω_{rN} (rad/s)	23	Rated generator speed ω_{gN} (rad/s)	23

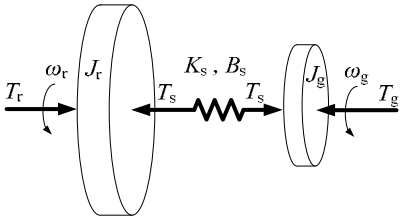

Fig.3 Two-mass model of the drive train

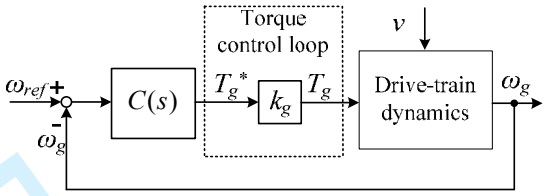

Fig.4 Simplified control block diagram of the WECS

rectification voltage) V_{dc} has a much slower dynamic than the dc-link current i_{dc}. From this point of view, the system configuration can be simplified as shown in Fig.4, in which $C(s)$ stands for the transfer function of speed regulator PI1 in Fig.1.

4). *entire WECS linear model and analysis*

Using small signal analysis to (2), (5)-(7) at a certain stable operational point $Q(V_Q, \omega_Q)$, the open-loop linear model of the WECS, with the inputs and outputs being $[\tilde{v} \quad \tilde{T}_g^*]^T$ and $[\tilde{T}_s \quad \tilde{\omega}_g]^T$ respectively, can be obtained as

$$\begin{bmatrix} \tilde{T}_s \\ \tilde{\omega}_g \end{bmatrix} = G(s) \begin{bmatrix} \tilde{v} \\ \tilde{T}_g^* \end{bmatrix} = \begin{bmatrix} G_{11}(s) & G_{12}(s) \\ G_{21}(s) & G_{22}(s) \end{bmatrix} \cdot \begin{bmatrix} \tilde{v} \\ \tilde{T}_g^* \end{bmatrix} \tag{8}$$

The detailed contents of $G(s)$ in (8) are given on Appendix I.

Hence, Fig.4 can be redrawn as Fig.5, from which the closed-loop transfer function from $[\tilde{v} \quad \tilde{\omega}_{ref}]^T$ to $[\tilde{T}_s \quad \tilde{\omega}_g]^T$ can be obtained as

$$\begin{bmatrix} \tilde{T}_s \\ \tilde{\omega}_g \end{bmatrix} = T(s) \begin{bmatrix} \tilde{v} \\ \tilde{\omega}_{ref} \end{bmatrix} = \begin{bmatrix} T_{11}(s) & T_{12}(s) \\ T_{21}(s) & T_{22}(s) \end{bmatrix} \cdot \begin{bmatrix} \tilde{v} \\ \tilde{\omega}_{ref} \end{bmatrix} \tag{9}$$

The detailed contents of $T(s)$ in (9) are given on Appendix II.

Known from the above analysis, due to the spatial distribution of the wind velocity, the effective wind velocity on the

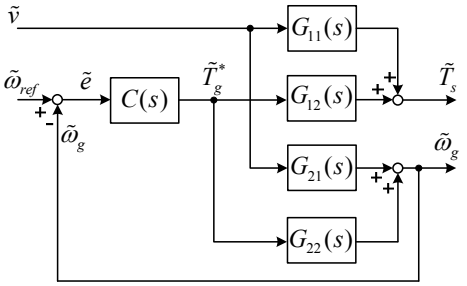

Fig.5 WECS linear model and control

rotor plane has a 3P oscillation component. This component will not only induce 3P torque ripple in aerodynamic torque according to (2), but also will make the drive-train bear 3P oscillation torque, defined as aerodynamic load, according to (9). The response of the closed-loop characteristics of aerodynamic load is determined by $T_{11}(s)$ in (9). Moreover, in this equation, $T_{12}(s)$ gives the response of the closed-loop characteristics of shaft torque caused by tracking the optimum generator speed reference, defined as transient load. Because generator speed control is a basic need in realizing power regulation, transient load is inevitable. Moreover, $T_{21}(s)$ and $T_{22}(s)$ determine the closed-loop performance of the generator speed under varying winds and generator speed reference respectively.

To know the response of the shaft torque better, the bode diagrams of the transfer functions $T_{11}(s)$, $T_{12}(s)$, $T_{21}(s)$ and $T_{22}(s)$ at 8m/s wind velocity are plotted in Fig.6. It is noticeable the existence of a poorly damped oscillation mode at about 8Hz. This mode will be excited by the aerodynamic load when the system operational condition changes due to wind or electrical load variations, potentially causing fatigue damage to the drive-train. In addition, speed oscillations will also be induced whenever the oscillation mode is exited, as shown in Fig.6 (d), causing flicker on the electric lines.

The most obvious approach to mitigate the oscillation magnitude of the generator speed is to slow down the response of generator speed, which can be achieved by reducing the gains of speed regulator $C(s)$. Note, however, that transfer function of $T_{11}(s)$ is lower-bounded by (find the expression of $T_{11}(s)$ in Appendix II)

$$|T_{11}(s)| \geq |G_{11}(s)| - |G_{21}(s)| \cdot |T_{12}(s)| \tag{10}$$

Whenever the generator speed response slows down (i.e. gains of $C(s)$ got reduced), $|T_{12}(s)|$ (or the transient load) becomes low according to the expression of $T_{12}(s)$ shown in Appendix II. One can then easily conclude from (10) that the aerodynamic load increases. Therefore, the transient load and the aerodynamic load compromise each other. As mentioned in section I, the source of this problem is the lack of damping in the system. Thus, the aerodynamic load and the vibration mode can be attenuated by adding external damping into the system.

III. Novel Aerodynamic Load Reduction Method

A. System inherent damping analysis

Usually, the wind-turbine inertia is much larger than that of

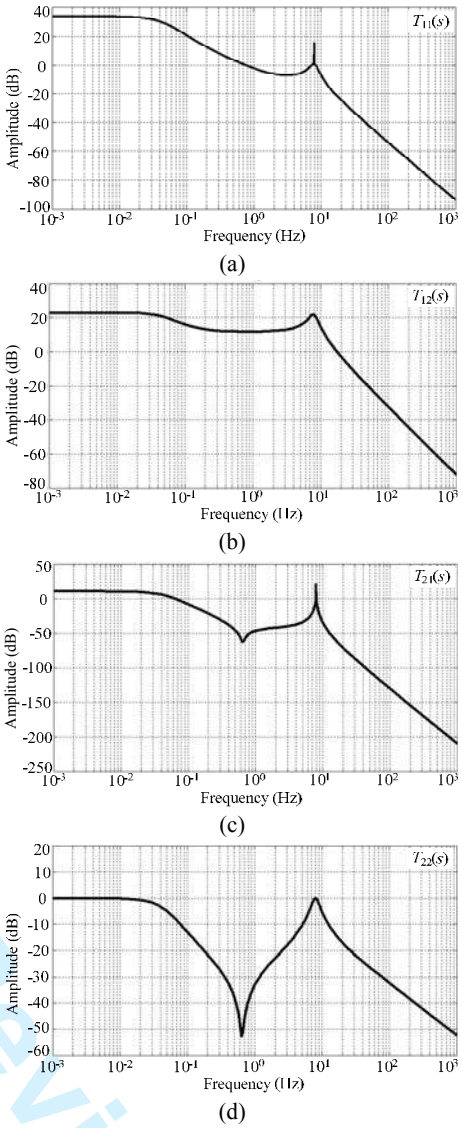

Fig.6 Closed-loop characteristics of the WECS: (a) $T_{11}(s)$; (b) $T_{12}(s)$; (c) $T_{21}(s)$; (d) $T_{22}(s)$.

the generator inertia ($J_r >> J_g$), so the dynamics of the rotor speed is much slower than that of the generator speed. Therefore, it is reasonable to assume the rotor speed to be constant compared with the generator speed dynamic. Based on this assumption, one can obtain the small signal model of (6) as

$$\dot{\tilde{\omega}}_r = \tilde{\omega}_g - \frac{K_s}{J_r}\tilde{\theta}_s \tag{11}$$

$$\dot{\tilde{\omega}}_g = \frac{K_s}{J_g}\tilde{\theta}_s - \frac{B_s}{J_g}\tilde{\omega}_g - \frac{1}{J_g}\cdot\frac{\partial T_g}{\partial \omega_g}\tilde{\omega}_g \tag{12}$$

$$\dot{\tilde{\theta}}_s = -\tilde{\omega}_g \tag{13}$$

$$\ddot{\tilde{\theta}}_s = \dot{\tilde{\omega}}_r - \dot{\tilde{\omega}}_g \tag{14}$$

From (11)-(14), the dynamic of the shaft electrical angle can be expressed as a second-order system

$$\ddot{\tilde{\theta}}_s + 2\xi\omega_n\dot{\tilde{\theta}}_s + \omega_n^2\tilde{\theta}_s = 0 \tag{15}$$

where

$$\omega_n = \sqrt{K_s(\frac{1}{J_r}+\frac{1}{J_g})} \tag{16}$$

$$\xi = \frac{B_s(J_r+J_g)}{2J_rJ_g\omega_n} + \frac{1}{2J_g\omega_n}\cdot\frac{\partial T_g}{\partial \omega_g} \tag{17}$$

In the above equation, notice that J_r>>J_g and ($\omega_n J_g$)>>B_s, (17) can be simplified as

$$\xi \approx \frac{1}{2J_g\omega_n}\cdot\frac{\partial T_g}{\partial \omega_g} \tag{18}$$

The system inherent damping is expressed in (18), which indicates that the inherent damping of the WECS is decided by the J_g, ω_n as well as the small-signal ratio of generator electrical torque with respect to generator speed ($\partial T_g/\partial\omega_g$). Because J_g, ω_n are intrinsic parameters of the system, they can't be modified once the system is selected. Alternatively, the only way to increase the system damping is to increase ($\partial T_g/\partial\omega_g$). It can be easily found out that a larger ($\partial T_g/\partial\omega_g$) results in a stronger damping effect. As a result, a compensation torque $T_{g,comp}$, which is proportional to the small signal value of the generator speed can be added in the generator torque loop to damp the aerodynamic load, as shown in Fig.7.

B. System analysis after damping injection

According to the above analysis, the compensation torque should be proportional to the small signal value of the generator speed, that is

$$T_{g,comp} = k_{comp}\tilde{\omega}_g \tag{19}$$

From Fig.7, we have

$$T_g = k_g T_g^* + k_{comp}\tilde{\omega}_g \tag{20}$$

Using small signal analysis to (2), (6) and (20) at the steady state $Q(V_Q, \omega_Q)$, the open-loop transfer function shown in (8) can be renewed as (21) after damping injection.

$$\begin{bmatrix}\tilde{T}_s\\ \tilde{\omega}_g\end{bmatrix} = G_d(s)\begin{bmatrix}\tilde{v}\\ \tilde{T}_g^*\end{bmatrix} = \begin{bmatrix}G_{11d}(s) & G_{12d}(s)\\ G_{21d}(s) & G_{22d}(s)\end{bmatrix}\cdot\begin{bmatrix}\tilde{v}\\ \tilde{T}_g^*\end{bmatrix} \tag{21}$$

where the expressions of $G_d(s)$ are shown in Appendix III.

Then, the system closed-loop transfer function can be obtained as

$$\begin{bmatrix}\tilde{T}_s\\ \tilde{\omega}_g\end{bmatrix} = T_d(s)\begin{bmatrix}\tilde{v}\\ \tilde{\omega}_{ref}\end{bmatrix} = \begin{bmatrix}T_{11d}(s) & T_{12d}(s)\\ T_{21d}(s) & T_{22d}(s)\end{bmatrix}\cdot\begin{bmatrix}\tilde{v}\\ \tilde{\omega}_{ref}\end{bmatrix} \tag{22}$$

where in (22), the transfer function $T_d(s)$ has similar expressions to $T(s)$, as shown in Appendix II. Notice should be taken that the expressions of $G(s)$ should be replaced with $G_d(s)$.

With the proposed active-damping scheme, the bode diagrams of the closed-loop transfer functions of the aerodynamic load and generator speed, known as $T_{11d}(s)$, $T_{12d}(s)$, $T_{21d}(s)$ and $T_{22d}(s)$, with different k_{comp} are plotted in Fig.8 under wind velocity 8m/s. One can see that not only the aerodynamic load has gotten a reduction without increasing the transient load, but also the system vibration mode can be dramatically reduced with the active damping scheme. The damping effect is stronger with a larger compensation gain. However, on the one hand, a new vibration mode at a lower frequency generates with larger compensation gains, as can be seen in Fig.8 (a). The aerodynamic load ultimately increases; on the other hand, the frequency response of the generator speed changes with the

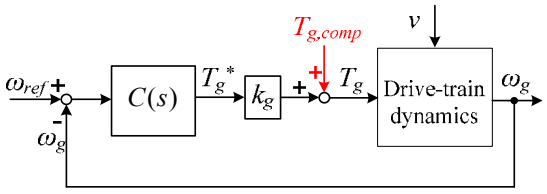

Fig.7 Control with damping injection

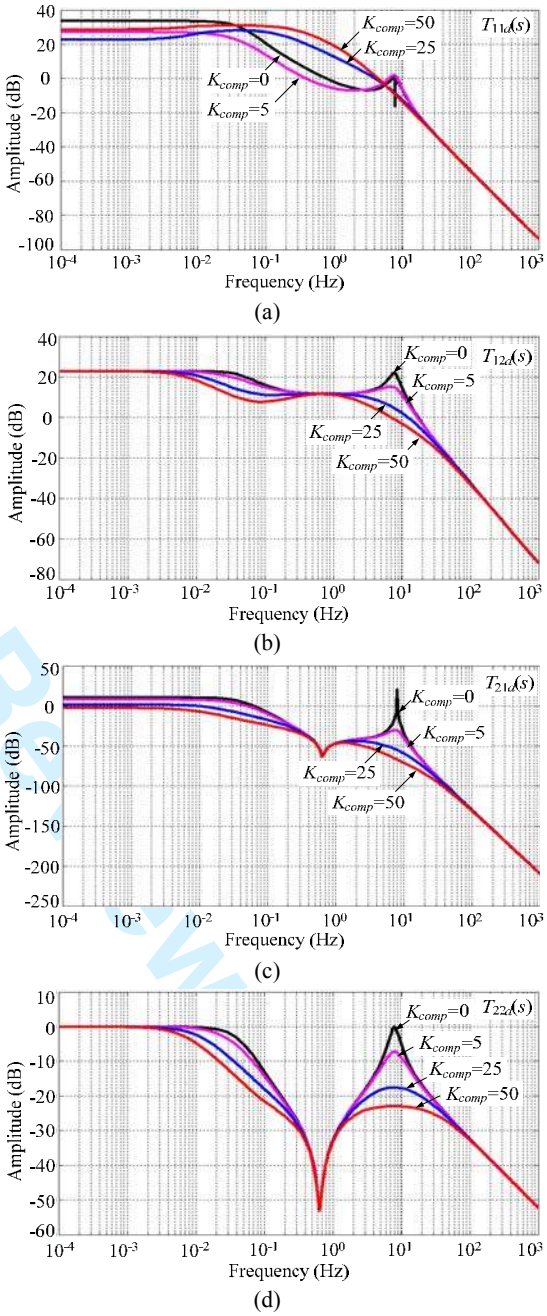

Fig.8 Closed-loop characteristics of the WECS: (a) $T_{11d}(s)$; (b) $T_{12d}(s)$; (c) $T_{21d}(s)$; (d) $T_{22d}(s)$.

compensator, and again, a larger compensation gain has a stronger effect. Hence, the choice of the compensation gain should consider the tradeoff between the damping effect and

the system response. Finally, the compensation strength is optimally chosen as k_{comp}=10 in this paper.

C. Way to obtain the small signal value of generator speed

Known from the above analysis, the system can be well damped if the compensation torque which is proportional to the small signal value of generator speed had been added in the torque control loop. However, the sensor used to detect the generator speed is usually an incremental encoder which continuously outputs the rotor position information. Therefore, it is difficult to get the small-signal value of the generator speed in the real application due to noise issues. Moreover, the rotor position cannot even be obtained in some speed sensorless WECS. In this case, other strategies should be considered for the identification of the small signal value of generator speed.

This paper declares that the generator speed information can be obtained from the electrical power flow, which provides the basis for the compensator implementation.

To the WECS studied in this paper, the power flow in the dc link can be expressed as follows:

$$V_{dc} i_{dc} = T_g \omega_g - P_{dc} \tag{23}$$

Again, notice the fact that the torque dynamic is much faster than the speed dynamic for a generator because of its large inertia. Ignoring the torque dynamic, (23) can be rewritten as

$$T_{gQ} \tilde{\omega}_g = V_{dc} i_{dc} - (T_{gQ} \omega_Q - P_{dc}) \tag{24}$$

In the power balanced control, the steady power flow ($T_{gQ}\omega_Q$ -P_{dc}) is equal to zero. Thus, (24) can be simplified as

$$\tilde{\omega}_g = \frac{V_{dc}}{T_{gQ}} \cdot i_{dc} \tag{25}$$

From (25), one can conclude that the small signal of generator speed is proportional to the dc-link capacitor current. That is to say, the small signal value of generator speed can be indirectly obtained through detecting the dc-link capacitor current. Then, combine (19) and (25), the damping injection method can be achieved.

IV. Experimental Verification

In order to verify the theoretical analyses, experimental results are given in this section. The experiments are done based on a 10kW PMSG-based direct-drive WECS laboratory test-rig setup shown in Fig.9. The experimental test-rig has a structure shown in Fig.1 and its control principle is a combination of Fig.1 and Fig.7. The system parameters are listed in Table. I. Regulator PI1 and PI2 are tuned through experiments and their proportional and integral gains are: K_{p1}=0.23, K_{I1}=0.18, K_{p2}=5, K_{I2}=20. During experiments, in order to facilitate the simulation of various wind environment, the wind turbine itself is emulated by a permanent magnet synchronous motor (PMSM) driving a PMSG. The PMSM, which has the same parameters with the PMSG, is driven by an inverter working in torque control mode, where the torque demand is given by the wind turbine simulator (WTS) based on a TMS320F2812 digital signal processor (DSP) from Texas Instruments (TI). The same turbine characteristic, as shown in Fig.2, is also programmed in the WTS to perfectly simulate the wind turbine's static and

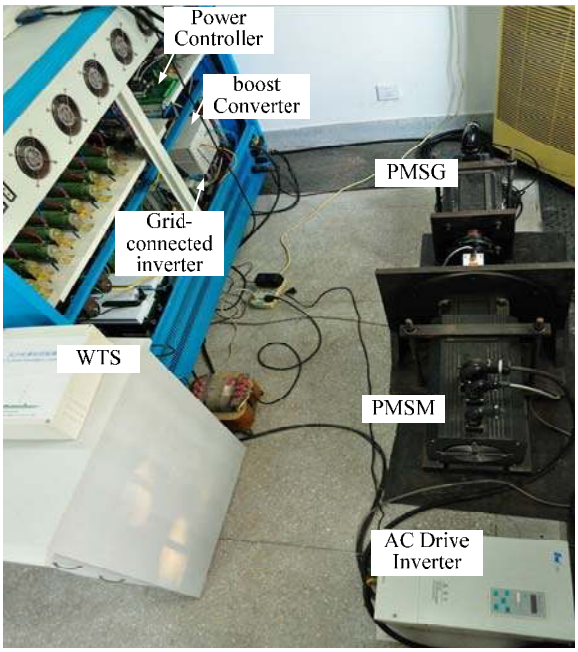

Fig.9 Laboratory test rig

dynamic performance. Particularly, the wind speed model used in chapter 3, reference [21] is adopted here to simulate the wind shear and tower shadow effects.

A. Operation without damping injection

In this experiment, the compensation torque is not added to the control loop, i.e. k_{comp}=0. Fig.10 and Fig.11 show the system responses. Fig.10 (a) plots a wind speed signal and its power spectrum density constructed with the adopted wind model. It can be clearly observed that the average wind speed is 7.5m/s and there is an energy concentration at about 8Hz (frequency of 3P for the average rotor speed can be calculated out as ω_r=16.8rad/s because the WECS is working in MPPT mode). As excited by this wind speed, The concentration of energy around frequency 8Hz in the aerodynamic torque can also be observed, as shown in Fig.10 (b). Since this vibration frequency is very close to the system natural resonant frequency determined by (16), the system natural resonant mode has been excited, causing high aerodynamic load and speed oscillations, as can be seen in Fig.10 (c) and (d). Not only makes the drive-train of the WECS more likely to be damaged by the high aerodynamic load, but also deteriorates the power quality and induces flickers on the electric lines.

What's more, it can be further noticed from Fig.11 that the low-frequency component of the dc-link current has the same frequency, phase angle, and trends with the generator speed, which keeps good pace with the theoretic analyses.

B. Operation with damping injection

The system responses with the proposed active-damping scheme under the same conditions are shown in Fig. 12 and 13. Still, because the wind contains high 3P resonant energy, 3P oscillation component in the aerodynamic torque can be found, as shown in Fig.12 (a). However, thanks to the generator torque compensation proposed, the oscillations in the shaft torque and generator speed are both dramatically damped (nearly 50dB),

as can be seen in Fig.12 (b) and (c). In addition, from Fig.13, it is noticed that there is no low-frequency oscillations appear in the generator speed and dc-link current any more. All the evidences show that the proposed method can indeed well damp the aerodynamic load and the system resonant mode.

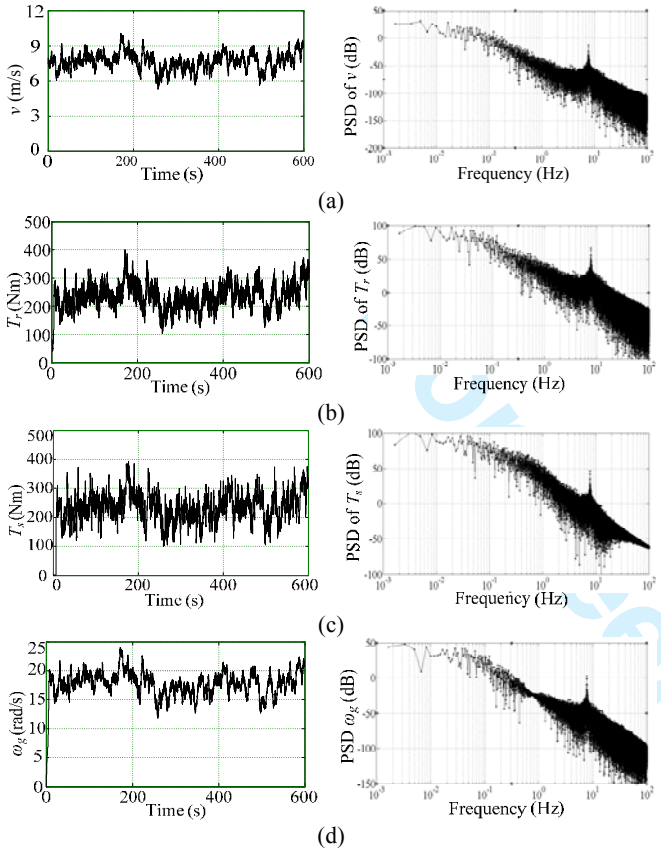

Fig.10 System response without damping injection: (a) wind velocity and its power spectrum density (PSD); (b) aerodynamic load and its PSD; (c) shaft torque and its PSD; (d) generator speed and its PSD.

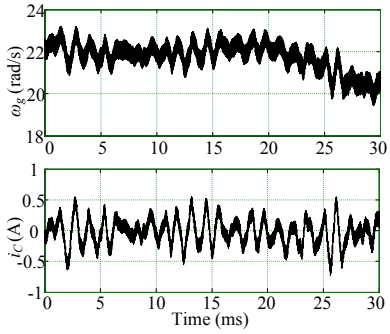

Fig.11 Relationship between the generator speed and capacitor current without damping injection

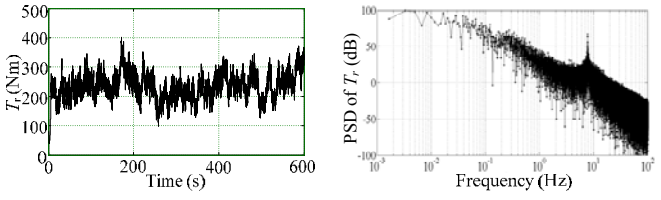

(a)

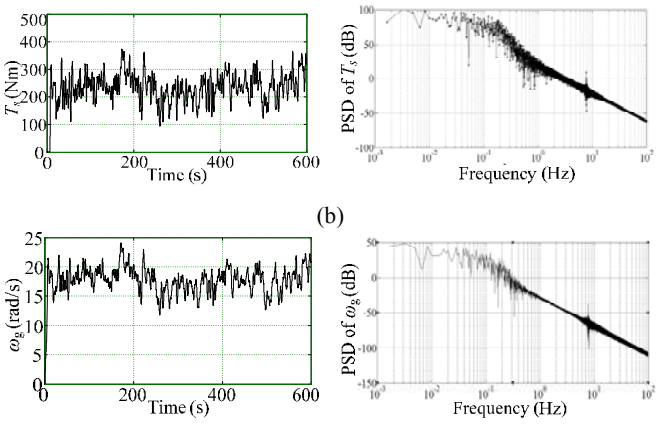

Fig.12 System response with damping injection: (a) aerodynamic load and its PSD; (b) shaft torque and its PSD; (c) generator speed and its PSD.

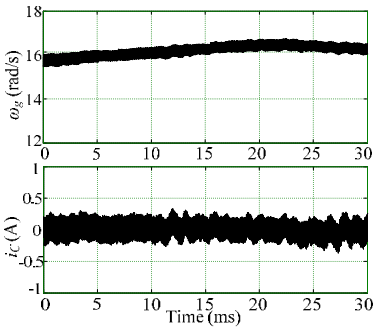

Fig.13 Relationship between the generator speed and capacitor current with damping injection

V. Conclusion

This paper mainly focuses on proposing a power control strategy to damp the serious aerodynamic load acting on the turbine shaft of PMSG-based direct-drive WECS. Through modeling analysis, the system inherent damping factor is firstly found out. The result shows that the inherent damping for this kind of WECS structure is very small and the system resonant mode is prone to be excited by the aerodynamic load. It is also found out that the oscillation information is contained in the dc-link capacitor current. Thus, the dc-link capacitor current is detected and applied to the compensation strategy which can provide positive damping to the system.

Appendix I
Expressions of $G(s)$ in (8)

$$G_{11}(s)=\frac{J_g\cdot k_r(v_Q,\omega_Q)}{B_r(v_Q,\omega_Q)}\cdot\frac{s(1-\frac{s}{z_0})}{d(s)} \tag{A1}$$

$$G_{12}(s)=-k_g\cdot\frac{(1-\frac{s}{z_0})(1-\frac{s}{z_1})}{d(s)} \tag{A2}$$

$$G_{21}(s)=\frac{k_r(v_Q,\omega_Q)}{B_r(v_Q,\omega_Q)}\cdot\frac{(1-\frac{s}{z_0})}{d(s)} \quad (A3)$$

$$G_{22}(s)=\frac{k_g}{B_r(v_Q,\omega_Q)}\cdot\frac{1+b_{q1}s+b_{q2}s^2}{d(s)} \quad (A4)$$

where in (A1)-(A4)

$$b_{q1}=\frac{B_s+B_r(v_Q,\omega_Q)}{K_s} \quad (A5)$$

$$b_{q2}=\frac{J_r}{K_s} \quad (A6)$$

$$z_0=-\frac{K_s}{B_s} \quad (A7)$$

$$z_1=-\frac{B_r(v_Q,\omega_Q)}{J_r} \quad (A8)$$

$$B_r(V_Q,\omega_Q)=\rho\pi R^4 k_T\left[R\cdot\omega_Q-\lambda_{\max}\cdot V_Q\right] \quad (A9)$$

$$k_r(V_Q,\omega_Q)=\rho\pi R^4 k_T\left[R\cdot\omega_Q-(1-\frac{C_{T\max}}{k_T\lambda_{\max}^2})\lambda_{\max}\cdot V_Q\right] \quad (A10)$$

and the $d(s)$ is

$$d(s)=1+a_1 s+a_2 s^2+a_3 s^3 \quad (A11)$$

Where in (A11), a_1, a_2 a_3 are determined by

$$a_1=\frac{K_s J_r+K_s J_g+B_s B_r(v_Q,\omega_Q)}{K_s B_r(v_Q,\omega_Q)} \quad (A12)$$

$$a_2=\frac{B_s J_r+B_s J_g+J_g B_r(v_Q,\omega_Q)}{K_s B_r(v_Q,\omega_Q)} \quad (A13)$$

$$a_3=\frac{J_r J_g}{K_s B_r(v_Q,\omega_Q)} \quad (A14)$$

APPENDIX II
EXPRESSIONS OF $T(S)$ IN (9)

$$T_{11}(s)=G_{11}(s)-\frac{G_{21}(s)G_{12}(s)C(s)}{1+G_{22}(s)C(s)} \quad (A15)$$

$$T_{12}(s)=\frac{G_{12}(s)C(s)}{1+G_{22}(s)C(s)} \quad (A16)$$

$$T_{21}(s)=\frac{G_{21}(s)}{1+G_{22}(s)C(s)} \quad (A17)$$

$$T_{22}(s)=\frac{G_{22}(s)C(s)}{1+G_{22}(s)C(s)} \quad (A18)$$

where regulator C(s) is chosen as

$$C(s)=\frac{0.23s+0.18}{s} \quad (A19)$$

APPENDIX III
EXPRESSIONS OF $G_d(S)$ IN (21)

$$G_{11d}(s)=\frac{k_r(v_Q,\omega_Q)\cdot k_{comp}}{\left[B_r(v_Q,\omega_Q)+k_{comp}\right]}\cdot\frac{(1-\frac{s}{z_0})(1-\frac{s}{z_2})}{d_1(s)} \quad (A20)$$

$$G_{12d}(s)=\frac{k_g\cdot B_r(v_Q,\omega_Q)}{\left[B_r(v_Q,\omega_Q)+k_{comp}\right]}\cdot\frac{(1-\frac{s}{z_0})(1-\frac{s}{z_1})}{d_1(s)} \quad (A21)$$

$$G_{21d}(s)=\frac{k_r(v_Q,\omega_Q)}{\left[B_r(v_Q,\omega_Q)+k_{comp}\right]}\cdot\frac{(1-\frac{s}{z_0})}{d_1(s)} \quad (A22)$$

$$G_{22d}(s)=\frac{k_g}{\left[B_r(v_Q,\omega_Q)+k_{comp}\right]}\cdot\frac{1+b_{q1}s+b_{q2}s^2}{d_1(s)} \quad (A23)$$

where in (A20)-A(23)

$$z_2=-\frac{k_{comp}}{J_g} \quad (A24)$$

$$d_1(s)=1+a_{1d}s+a_{2d}s^2+a_{3d}s^3 \quad (A25)$$

and

$$a_{1d}=\frac{K_s(J_r+J_g)+k_{comp}\left[B_s+B_r(v_Q,\omega_Q)\right]+B_s B_r(v_Q,\omega_Q)}{K_s\left[B_r(v_Q,\omega_Q)+k_{comp}\right]} \quad (A26)$$

$$a_{2d}=\frac{J_r(B_s+k_{comp})+J_g K_s\left[B_r(v_Q,\omega_Q)+B_s\right]}{K_s\left[B_r(v_Q,\omega_Q)+k_{comp}\right]} \quad (A27)$$

$$a_{3d}=\frac{J_r J_g}{K_s\left[B_r(v_Q,\omega_Q)+k_{comp}\right]} \quad (A28)$$

REFERENCES

[1] Li H, and Chen Z, "Overview of different wind generator systems and their comparisons," *IET Renewable Power Generation*, vol.2, pp.123-128, 2008.

[2] Liserre, M., Cárdenas, R., Molinas, M., Rodriguez, J., "Overview of multi-MW wind turbines and wind parks," *IEEE Transactions on Industrial Electronics*, vol.58, pp.1081-1095, 2011.

[3] A.A. El-Sattar, N.H. Saad, M.Z. Shams El-Dein, "Dynamic response of doubly fed induction generator variable speed wind turbine under fault," *Electric Power Systems Research*, vol.78, pp. 1240-1246, 2008.

[4] Johannes H. J. Potgieter, and Maarten J. Kamper, "Torque and voltage quality in design optimization of low-cost non-overlap single layer winding permanent magnet wind generator," *IEEE Transitions on Industrial Electronics*, vol.59, No.5, pp.2147-2156, 2012.

[5] H. Polinder, F. F. A. Van der Pijl, G. J. de Vilder, and P. J. Tavner, "Comparison of direct-drive and geared generator concepts for wind turbines," *IEEE Trans. Energy Conversion*, vol. 3, no. 21, pp. 725–733, Sep. 2006.

[6] Fernando D. Bianchi, Hernan De Battista, Ricardo J. Mantz, "Wind turbine control systems principles, modeling and gain scheduling design," *Springer-Advances in Industrial Control Series*, 2006.

[7] Dale S. L. Dolan, Peter W. Lehn, "Simulation model of wind turbine 3p torque oscillations due to wind shear and tower shadow," *IEEE Transactions on Energy Conversion*, vol. 21, No.3, pp: 717-724, 2006.

[8] A. Hansen, G. Michalke, P. Sørensen, T. Lund, and F. Iov, "Coordinated voltage control of DFIG wind turbines in uninterrupted operation during grid faults," *Wind Energy*, vol. 10, No. 1, pp: 51–68, 2007.

[9] S. Brownlees, B. Fox, D. Flynn, and T. Littler, "Wind farm induced oscillations," in *Proc. 41st Int. UPEC*, vol. 1, pp: 118–122, 2006.

[10] S. Jockel, B. Hagenkort, T. Hartkopf, and H. Schneider, "Direct-drive synchronous generator system for offshore wind farms with active drive train damping by blade pitching," in *Proc. EWEC*, 2001, pp: 991–994.

[11] M. Bierhoff and F. Fuchs, "Active damping for three-phase PWM rectifiers with high-order line-side filters," *IEEE Transactions on Industrial Electronics*, vol. 56, no. 2, pp: 371–379, 2009.

[12] M. S. El-Moursi, B. Bak-Jensen, and M. H. Abdel-Rahman, "Novel STATCOM controller for mitigating SSR and damping power system oscillations in a series compensated wind parks," *IEEE Trans. Power Electron.*, vol. 25, no. 2, pp: 429–441, 2010.

[13] R. Varma, S. Auddy, and Y. Semsedini, "Mitigation of subsynchronous resonance in a series-compensated wind farm using FACTS controllers," *IEEE Trans. Power Del.*, vol. 23, no. 3, pp: 1645–1654, 2008.

[14] B. Rigby, N. Chonco, and R. Harley, "Analysis of a power oscillation damping scheme using a voltage-source inverter," *IEEE Transactions on Industrial Applications.*, vol. 38, no. 4, pp: 1105–1113, 2002.

[15] Geng Hua, Xu Dewei, Wu Bin and Yang Geng, "Active damping for tortional vibrations in PMSG based WECS," *in 5th IEEE Applied Power Electronics Conference and Exposition*, pp: 2126–2131, 2010.

[16] Ranjan Vepa, "Nonlinear, optimal control of a wind turbine generator," *IEEE Transactions on Energy Conversion*, vol.26, No.2, pp: 468-478, 2010.

[17] I. Serban, C. Marinescu, "A sensorless control method for variable-speed small wind turbines," *Renewable Energy*, vol.43, pp: 256-266, 2010.

[18] Yuanye Xia, Khaled H. Ahmed, and Barry W. Williams, "A new maximum power point tracking technique for permanent magnet synchronous generator based wind energy conversion system," *IEEE Transaction on Power Electronics*, vol.26, No.12, pp: 3609-3620, 2011.

[19] Haque M.E., Negnevitsky M., and Muttaqi K.M., "A novel control strategy for a variable-speed wind turbine with a permanent-magnet synchronous generator," *IEEE Transaction on Industrial Applications*, vol.46, pp.331-339, 2010.

[20] S. Muyeen, M. Ali, R. Takahashi, T. Murata, J. Tamura, Y. Tomaki, A. Sakahara, and E. Sasano, "Comparative study on transient stability analysis of wind turbine generator system using different drive train models," *IET Renewable Power Generation*, vol. 1, pp: 131–141, 2007.

[21] Pedro Rosas, "Dynamic influences of wind power on the power system. Kongens Lyngby," Ph. D. Dissertation, Denmark, Technical University of Demark, 2003.

Reply to Reviewers' Comments on Paper No. 13-TIE-1170

■ **Title: "On Optimizing the Aerodynamic Load Acting On the Turbine Shaft of PMSG-Based Direct-Drive Wind Energy Conversion System "**

We wish to thank the Associated Editor and all the reviewers for their time and valuable comments on our paper. We have made necessary changes in the paper and the answers in accordance with the comments required by the reviewers. Below the comments are reprinted and followed by the corresponding answers in green color. In the revised paper, the yellow color is used for highlighting the changed parts.

➢ Reply to the AE's Comments

Comments to the Author:

The reviewers have highlighted the major shortcomings of this paper and I agree with their opinion. Moreover, the paper seems to contain little novelty if compared to the previous work of the authors.

Answer: Thank you for your kind comment. The purpose of this paper is to propose a power control method to attenuate the aerodynamic load acting on the turbine shaft. In the authors' opinion, the novelties of this paper are: 1. The closed-loop performance of the aerodynamic load has been deeply analyzed through modeling analysis, this is different from the previous works; 2. The relationship between the performances of the aerodynamic load and transient load has been found out. The reason why the aerodynamic load can't be attenuated by simply adjusting the PI controller is pointed out; 3. Because the diode rectifier rather than the PWM rectifier is adopted in this paper, large current harmonics exist in the generator phase current. The generator torque control can't be realized through controlling the q-axis current like the circumstance if the PWM rectifier had been adopted. This makes injecting damping into the power control system more complicated. Ways to adjust the generator torque and achieve damping injection under this circumstance are discussed in this paper; 4. The power signal spectrum analysis is made in this paper to clearly show the performances of the turbine with and without the damping injection. The effects of the proposed power control method are directly shown to the readers. 5. Impact on the system efficiency is discussed in this paper.

Also, the authors made necessary changes to the paper according to the reviews' comments. Details are shown in the answers to the reviews' comments shown in the following.

➢ Reply to First Reviewer

Comments to the Author:

Comment 1

In my humble opinion this paper should more plainly stress the differences with previous works, specially Hua Geng; Xu, D.; Bin Wu; Geng Yang, "Active Damping for PMSG-Based WECS With DC-Link Current Estimation," Industrial Electronics, IEEE Transactions on , vol.58, no.4, pp.1110-1119, April 2011. It is indicated that the intended contribution of the paper is to demonstrate the difficulty to damp the aerodynamic load and suppress the oscillations. However, the aerodynamics are studied using the curves shown in Fig. 2 which are clearly static so they cannot "perfectly simulate the wind turbine's dynamic performance" as it is stated in page 6, line 60, left.

Answer: Thank you for your kind comments. In the authors' opinion, the research focus of our paper is quite different from the paper you referenced, mainly on: 1. This paper focuses on attenuating the

aerodynamic load acting on the turbine shaft caused by the blades' rotational sampling to the spatial distribution winds. The closed-loop performance of the aerodynamic load has been obtained through modeling analysis in our paper. Moreover, the relationship between the performances of the aerodynamic load and transient load has also been found out. The reason why the aerodynamic load can't be attenuated by simply adjusting the gains of the PI controller is pointed out; 2. Unlike the referenced paper, the diode rectifier rather than the PWM rectifier is adopted in this paper. Because of the commutation over-lapping phenomenon of the diode rectifier, large current harmonics exist in the generator phase current. The generator torque control can't be realized through controlling the *q*-axis current like the circumstance if the PWM rectifier had been adopted. This makes injecting damping into the power control system more complicated. Ways to adjust the generator torque and achieve damping injection under this circumstance are discussed in this paper; 3. The power signal spectrum analysis is made in this paper to clearly show the performances of the turbine with and without the damping injection. The effects of the proposed power control method are directly shown to the readers. 4. Impact on the system efficiency is discussed in this paper.

To the problem that using Fig.2 cannot "perfectly simulate the wind turbine's dynamic performance", the question comes to whether the wind turbine emulator can be used to replace the real wind turbine or not. Fig. i illustrates the equivalent diagrams of two wind energy conversion systems using actual wind turbine and wind turbine emulator respectively. The motion equation of these two systems can be written as

$$T_r / n = (J_r / n^2 + J_g)\mathrm{d}\omega_{g1} / \mathrm{d}t + T_e \tag{1}$$

$$T_m = (J_m + J_g)\mathrm{d}\omega_{g2} / \mathrm{d}t + T_e \tag{2}$$

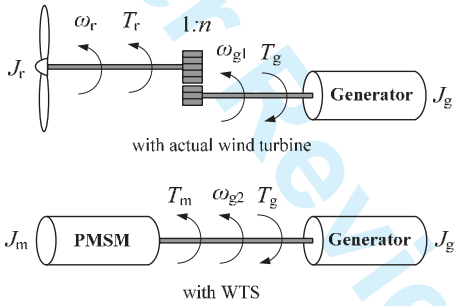

Fig.i Equivalent diagram of WECSs using actual wind turbine and WTS as power source

To ensure both the static and transient behavior of the actual wind turbine and wind turbine emulator are the same, what we need to do is to set ω_{g2} equals to ω_{g1} (using ω to stand for the same value). Then, by replacing ω_{g1} and ω_{g2} with ω in (1) and (2), we can obtain the real-time torque reference that the motor has to generate in order to replace the real turbine,

$$T_m = T_r / n - (J_r / n^2 - J_m)\mathrm{d}\omega / \mathrm{d}t \tag{3}$$

And according to the aerodynamics, the aerodynamic torque of the turbine can be expressed as

$$T_r = 0.5\pi\rho C_T(\lambda, \beta)R^3 v^2 \tag{4}$$

Tip-speed-ratio λ is determined by

$$\lambda = \omega R / v \tag{5}$$

Hence, through detecting the generator speed ω and wind velocity v (v is giving by the WTS) and combining the C_T-λ curve shown in Fig.2, the aerodynamic torque T_r of the real wind turbine can be calculated using (4). Therefore, the torque that the PMSM is required to generate can be obtained using (3).

Driving by this torque, the generator speed is just equal to that driving by the real wind turbine. Thus, the wind turbine emulator can be used to replace the real wind turbine. In addition, a reference about the operational principle of the wind turbine emulator is added in the revised paper, as referred to [21].

(Previous sentences on Page 6, from line 59 on the left column)

The same turbine characteristic, as shown in Fig.2, is also programmed in the WTS to perfectly simulate the wind turbine's static and dynamic performance.

(Modified sentence)

The same turbine characteristic, as shown in Fig.2, is also programmed in the WTS to perfectly simulate the wind turbine's static and dynamic performance. The correctness of the WTS is verified in the previous work [21].

Comment 2

Regarding to the experimental results:

- The generator speed in Fig. 10 oscillates around 18 rad/s whereas in Fig. 11 it does around 22 rad/s, when the studied situation is supposed to be the same. In Fig. 13, with damping injection, the speed is lower and oscillates around 16 rad/s.
- It is difficult understand how two different experiments provide so similar results. Differences in shaft torque and generator speed in Figs. 10 and 12 are almost invaluable.

Answer: Thank you for your kind comment. Fig.10 (d) depicts the generator speed without damping injection. From the PSD of the generator speed, we can see that the generator speed oscillates at about 8Hz=50.3rad/s, this is equal to the natural resonant frequency of the system. In Fig.11, the authors failed to correctly mark the time axis in editing process. The correct timescale is 0.5s/div. This mistake also appears in Fig.13. In the revised paper, it is modified.

In addition, the experiments with and without damping injection are done under the same circumstances using the same experimental platform. The only difference is that the compensation torque is added to the control system when the external damping is injected. However, because the wind profile can not be the same in two experiments because of its random characteristics, PSD analysis is employed to facilitate the comparative study. Because the wind velocity has energy concentration at about 8Hz, which is around the natural resonant frequency, there must have an energy concentration at 8Hz in the aerodynamic torque regardless of the damping injection method according to equation (2) in the previous paper. Thus, in Fig.10 (b) and Fig.12 (a), energy concentration can be noticed at 8Hz. If the damping injection had been adopted, the oscillations in shaft torque (aerodynamic load) and generator speed were both dramatically damped, as can be seen in Fig.12(b) and (c). The experimental results are quite different compared with Fig.10 (c) and (d). Thus, the authors think the experimental results are reasonable and correct.

(Previous Fig.11 and Fig.13)

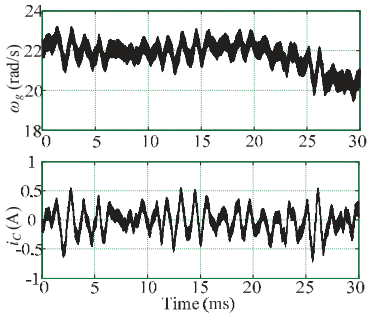

Fig.11 Relationship between the generator speed and capacitor current without damping injection

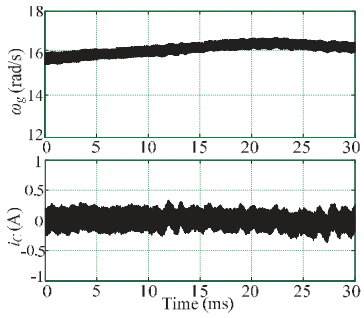

Fig.13 Relationship between the generator speed and capacitor current with damping injection

(Revised Fig.11 and Fig.13)

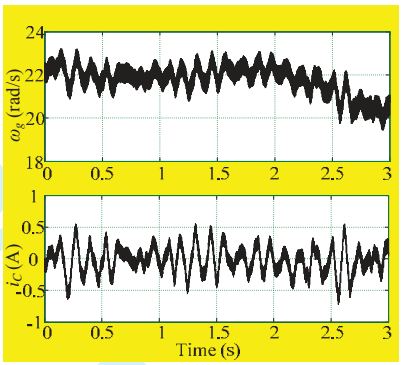

Fig.11 Relationship between the generator speed and capacitor current without damping injection

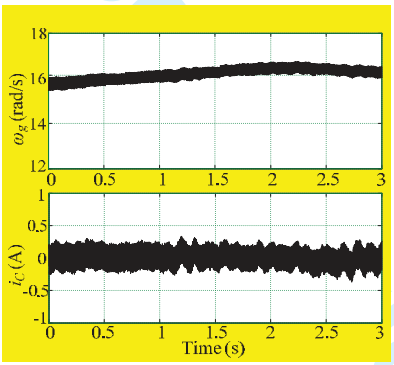

Fig.13 Relationship between the generator speed and capacitor current with damping injection

Comment 3

On the other hand, there are some mistakes in the nomenclature, lambda_max is omitted, k_comp is in capitals and also some typos and grammatical errors throughout the text. For example:

"convert" in page 2, lines 46 and 48, right.

"leads" in page 2, line 13, left.

"with damping injection proposed." in page 2, line 46, left.

"becomes low according" in page 4, line 49, left.

"various wind environment" in page 6, line 53, left.

"the same parameters with the PMSG" in page 6, line 56, left.

"by this wind speed, The concentration" in page 6, line 40, right.

"there is no low-frequency oscillations appear in the generator" in page 7, line 5, left.

Finally, the sentence "Consider the fact that the..." beginning at page 2, line 30, requires better drafting.

Answer: Thank you for your kind comment. Firstly, the authors add the missing definitions used in the full text in the nomenclature. Then, the authors have rechecked the paper for a few times and revised some bad expressions, grammar mistakes and some puzzled sentences. Also, this paper is sent to a student who is majored in English Language for a double check before resubmission. Generally, attempts are done to improve the quality of this paper as much as possible. The revisions in the revised paper are listed in the following.

(Page 1, Line 59 on the left column)

K_{comp} is modified to k_{comp}. Correspondingly, k_{comp} in Fig.8 has been modified.

(Previous Fig.8)

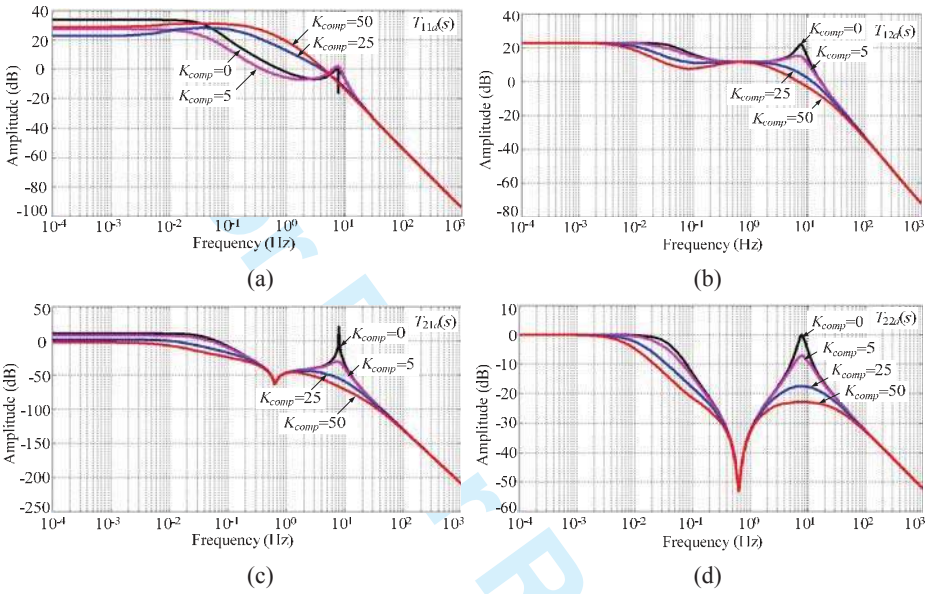

Fig.8 Closed-loop characteristics of the WECS: (a) $T_{11d}(s)$; (b) $T_{12d}(s)$; (c) $T_{21d}(s)$; (d) $T_{22d}(s)$.

(Modified Fig.8)

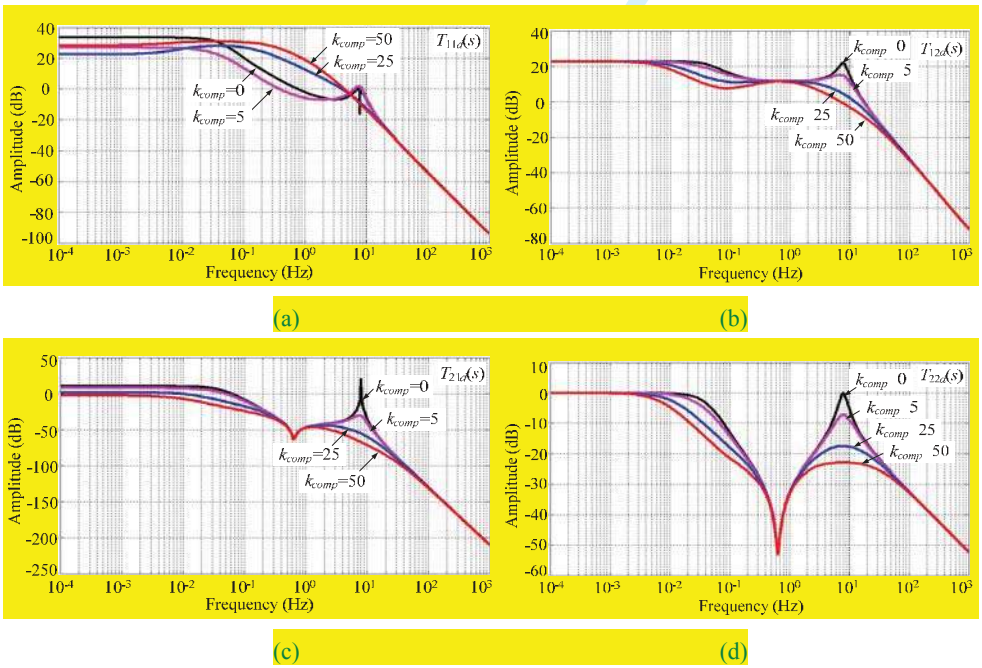

Fig.8 Closed-loop characteristics of the WECS: (a) $T_{11d}(s)$; (b) $T_{12d}(s)$; (c) $T_{21d}(s)$; (d) $T_{22d}(s)$.

(Previous sentence on Page 1, Line 26 on the left column)

Both the aerodynamic load and the system inherent resonant mode can be well damped if the proposed method had been adopted.

(Modified sentence)

Both the aerodynamic load and the system's inherent resonant mode could be well damped if the proposed method were adopted.

(Previous sentences on Page 1, Line 44 on the right column)

The system energy generation process can be typically synthesized as: the wind turbine captures the power from wind by means of turbine blades and convert it to mechanical power. The PMSG is driven by the rotating turbine through the drive-train and convert the energy from mechanical to electrical.

(Modified sentences)

The system energy generation process can be typically synthesized as: the wind turbine captures the power from wind by means of turbine blades and converts it to mechanical power. The PMSG is driven by the rotating turbine through the drive-train and converts the energy from mechanical to electrical.

(Previous sentence on Page1, Line 55 on the right column)

In addition, to a horizontal wind turbine, the airflow in front of the tower is forced to bypass it, making the airflow take a lateral speed whereas its axial speed decreases, called tower shadow effect [6].

(Modified sentence)

In addition, to a horizontal wind turbine, the airflow in front of the tower is forced to bypass it, making the airflow take a lateral speed whereas its axial speed decreases, and this is called tower shadow effect [6].

(Previous sentence on Page2, Line 46 on the left column)

The intended contribution of this paper is to demonstrate that the difficulty to damp the aerodynamic load and suppress the oscillations can be achieved by a power control strategy with damping injection proposed.

(Modified sentence)

The intended contribution of this paper is to demonstrate that the difficulty in damping the aerodynamic load and suppressing the oscillations can be achieved by using a power control strategy proposed.

(Previous sentence on Page2, Line 25 on the right column)

To balance the generated power and the power injected into the grid, the dc-bus voltage V_l is usually controlled stable by the inverter [16]-[17].

(Modified sentence)

To balance the generated power and the power injected into the grid, the dc-bus voltage V_l is usually stabilized by the inverter [16]-[17].

(Previous sentence on Page2, Line 44 on the right column)

This method first separates the whole system into several interconnected subsystems and then modeling each subsystem so as to obtain the entire system model.

(Modified sentence)

This method first separates the whole system into several interconnected subsystems and then models each subsystem so as to obtain the entire system model.

(Previous sentence on Page4, Line 48 on the left column)

Whenever the generator speed response slows down (i.e. gains of $C(s)$ got reduced), $|T_{12}(s)|$ (or the transient load) becomes low according to the expression of $T_{12}(s)$ shown in Appendix II.

(Modified sentence)

Whenever the generator speed response slows down (i.e. gains of $C(s)$ is reduced), $|T_{12}(s)|$ (or the transient load) decreases according to the expression of $T_{12}(s)$ shown in Appendix II.

(Previous sentences on Page 6, from line 51 on the left column)

During experiments, in order to facilitate the simulation of various wind environment, the wind turbine itself is emulated by a permanent magnet synchronous motor (PMSM) driving a PMSG. The PMSM, which has the same parameters with the PMSG, is driven by an inverter working in torque control mode, where the torque demand is given by the wind turbine simulator (WTS) based on a TMS320F2812 digital signal processor (DSP) from Texas Instruments (TI).

(Modified sentences)

During experiments, in order to apply different kinds of wind velocities to the WECS, the wind turbine itself is emulated by a permanent magnet synchronous motor (PMSM) driving a PMSG. The parameters of the PMSM are the same to the PMSG. The PMSM is driven by an inverter working in torque control mode, where the torque demand is given by the wind turbine simulator (WTS) based on a TMS320F2812 digital signal processor (DSP) from Texas Instruments (TI).

(Previous sentence on Page 6, line 39 on the right column)

As excited by this wind speed, The concentration of energy around frequency 8Hz in the aerodynamic torque can also be observed, as shown in Fig.10 (b).

(Modified sentence)

When this wind velocity is applied to the WECS, the energy concentration at around 8Hz in the aerodynamic torque can also be observed, as shown in Fig.10 (b).

(Previous sentence on Page 6, line 45 on the right column)

Not only makes the drive-train of the WECS more likely to be damaged by the high aerodynamic load, but also deteriorates the power quality and induces flickers on the electric lines.

(Modified sentence)

It not only makes the drive-train of the WECS more likely to be damaged by the high aerodynamic load, but also deteriorates the power quality and induces flickers on the electric lines.

(Previous sentences on Page 7, line 5 on the left column)

In addition, from Fig.13, it is noticed that there is no low-frequency oscillations appear in the generator speed and dc-link current any more.

(Modified sentence)

In addition, the low-frequency oscillations of generator speed and dc-link current can not be observed anymore in Fig.13.

➢ **Reply to Second Reviewer**

Comments to the Author:

Comment 1

- The choice of PMSG with direct attack is not justified for this study

Answer: Thank you for your comment. The PMSG based direct-drive WECS is chosen as the research object in this paper mainly for two reasons: A. This type of turbine structure features high reliability because of the possibility of cancellation of gearbox and good fault ride through ability. It is widely treated as a promising and preferred turbine structure. B. The drive-train shaft of the multi-pole PMSG-based WECS is rather "soft" and prone to oscillation. There are researches show that the larger the power level, the softer the drive-train shaft. Therefore, it is necessary to do research on how to damp the aerodynamic load and suppress the oscillations.

Comment 2

- The proposed system Fig 1.- is limited for wind high speeds

Answer: Thank you for your good comment. Because the fixed-pitch wind turbine is adopted in the paper, at high wind velocities, passive stall control should be applied to the system. In the authors' previous publication listed below, the overall power control strategy had been studied. The power of the WECS can be well regulated from cut-in wind velocity to cut-out wind velocity using the method proposed in that paper. This reference is added in the revised paper, and the control strategy at high wind velocities is added in Fig.1. The readers can then become clear by how the overall power is regulated now.

(Previous Fig.1)

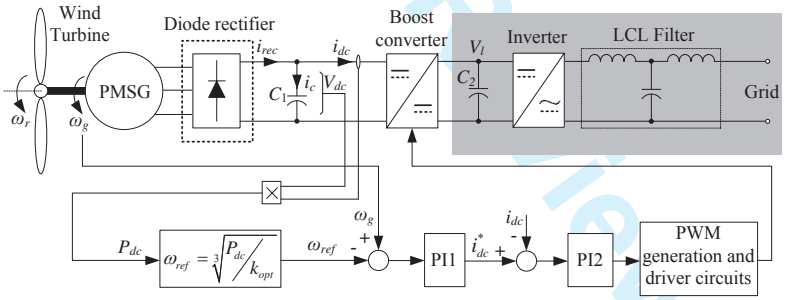

Fig.1 System configuration of the adopted 10kW PMSG-based direct-drive variable-speed WECS

(Modified Fig.1)

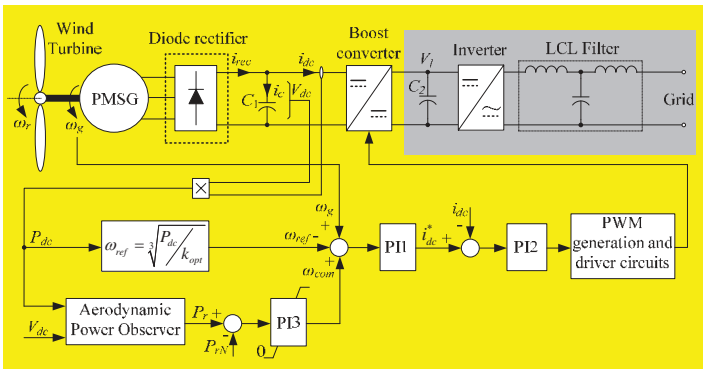

Fig.1 System configuration of the adopted 10kW PMSG-based direct-drive variable-speed WECS

Added reference: [18] Jiawei Chen, Jie Chen, Chunying Gong, "New overall power control strategy for variable-speed fixed-pitch wind turbines within the whole wind velocity range," IEEE Transactions on Industrial Electronics, vol.60, no.7, pp: 2652-2660, 2013.

(Previous sentences on Page 2, from line 29 to 37 on the right column)

Meanwhile, the power optimization is achieved by introducing the well known power feedback control method into the control system, as shown in the lower part of Fig.1 [18]-[19]. In this method, the output power of the turbine P_{dc} is firstly sensed and used to calculate the optimum generator speed reference according to the pre-learned aerodynamic characteristics. If the generator speed is controlled to follow this optimum reference very well, the output power can be easily optimized.

(Modified sentences)

Meanwhile, the overall power optimization is achieved by introducing the well known power feedback maximum power point tracking (MPPT) control method into the control system at low wind velocities and the passive soft-stalling control strategy at above rated wind velocities [18]-[19], which is shown in the lower part of Fig.1. In low wind velocity region, the output power of the turbine P_{dc} is firstly sensed and used to calculate the optimum generator speed reference according to the pre-learned aerodynamic characteristics. If the generator speed is controlled to follow this optimum reference very well, the output power can be easily optimized. Whenever the wind velocity exceeds rated value, a generator speed compensation signal ω_{com} generates and is added to the speed control loop, aiming to reduce the generator speed, further to limit the power of the WECS. The operational principle can be referred to [18].

Comment 3

The electric parameters of the permanent magnet synchronous machines for the bench test are not given

Answer: Thank you for your kind comment. The electrical parameters of the PMSG are added in Table.1 in the revised paper.

(Previous Table.1)

TABLE I PARAMETERS OF WECS

Parameters of the turbine	Value	Parameters of the PMSG	Value
Radius of the turbine R (m)	3.7	Shaft stiffness K_s (N·m/rad)	620
Numbers of blades	3	Friction Coefficient B_s (N·m·s/rad)	0.14
Moment of inertia of the blade J_r (kg·m^2)	38	Moment of inertia of the generator J_g (kg·m^2)	0.32
Rated rotor power P_{rN} (kW)	10	Rated output power P_{dcN} (kW)	10
rated wind velocity V_N (m/s)	10.5	Permanent Magnet Flux ψ (wb)	1.28
Max power coefficient C_{pmax}	0.35	Rated rotor speed ω_N (RPM)	500
Optimum tip-speed-ratio λ_{opt}	8.2	Winding Resistance R_s (Ω)	3.6
Rated rotor speed ω_{rN} (rad/s)	23	Rated generator speed ω_{gN} (rad/s)	23

(Modified Table.1)

TABLE I PARAMETERS OF WECS

Parameters of the turbine	Value	Parameters of the PMSG	Value
Radius of the turbine R (m)	3.7	Number of pole-pairs	8
Numbers of blades	3	Moment of inertia of the generator J_g (kg·m^2)	0.32
Moment of inertia of the blade J_r (kg·m^2)	38	Rated output power P_{dcN} (kW)	12
Rated rotor power P_{rN} (kW)	10	Permanent Magnet Flux ψ (wb)	1.28
rated wind velocity V_N (m/s)	10.5	Rated generator speed ω_{gN} (rad/s)	23
Max power coefficient C_{pmax}	0.35	Winding Resistance R_s (Ω)	1.2
Optimum tip-speed-ratio λ_{opt}	8.2	Winding inductance L (mH)	3.6
Rated rotor speed ω_{rN} (rad/s)	23	Rated output voltage (rectified to DC) V_{dcN} (V)	320
Shaft stiffness K_s (N·m/rad)	620	Friction Coefficient B_s (N·m·s/rad)	0.14

Comment 4

The study of the overall efficiency must be done

Answer: Thank you for your good comment. In the revised paper, in section IV, a third part on analyzing the system overall efficiency with and without damping injection is added.

(Added parts in Section IV)

C. System efficiency analysis with and without damping

From the above analysis, one can get to know that the proposed damping injection method can help attenuate the serious aerodynamic load. In this section, study is carried out on the system efficiency. The research focus is mainly laid on whether the system efficiency will be affected or not if the damping injection method had been adopted.

The power variations with respect to the wind velocity before and after adopting the damping injection method are plotted in Fig.14. And the variations of power coefficients on these two conditions are also plotted in Fig.15. From Fig.15, it can be observed that though higher power coefficient falling appears after using the proposed damping injection method, it is not much. From Fig.14, one can see that the power variations on both conditions follow the same pattern and are very close to each other. This evidence shows that the proposed method has little impact on the system overall efficiency. Besides, a decreasing in power variations can be observed in Fig.14. This indicates that the proposed method features smaller power oscillation.

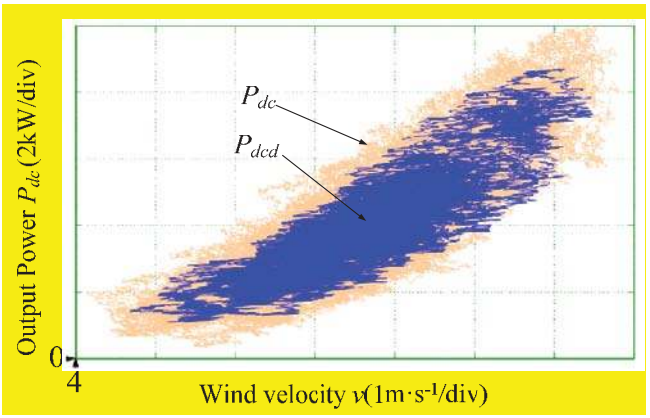

Fig.14 Output power of the WECS versus wind velocity. P_{dc} stands for the output power without damping and P_{dcd} strands for that with damping.

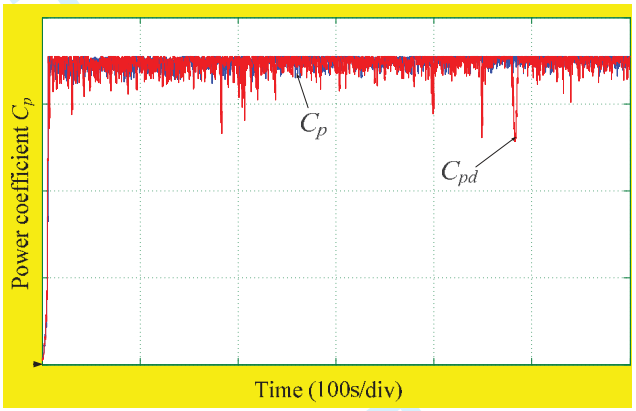

Fig.15 Power coefficient curve. C_p stands for the power coefficient without damping and C_{pd} strands for that with damping.

➢ **Reply to EIC's Comments**

Comments to the Author:

Manuscripts must be technically linked with some other recently published papers of the journal where the manuscript is submitted to.

Answer: Thank you for your kind comment. From the latest journal publications you attached, below references were updated.

[1] Xu She, Huang A.Q., Fei Wang, Burgos R., "Wind energy system with integrated functions of active power transfer, reactive power compensation, and voltage conversion," *IEEE Transactions on Industrial Electronics*, vol.60, no.10, pp.4512- 4524, 2013.

[2] Barote L., Marinescu C., Cirstea M.N., "Control structure for single-phase stand-alone wind-based energy sources," *IEEE Transactions on Industrial Electronics*, vol.60, no.2, pp: 764-772, 2013.

[3] Thanh Hai Nguyen, Dong-Choon Lee, "Advanced fault ride-through technique for PMSG wind turbine systems using line-side converter as STACOM," *IEEE Transactions on Industrial Electronics*, vol.60, no.7, pp: 2842~2850, 2013.

[4] Arani M.F.M., EI-Saadany E.F., "Implementing virtual inertia in DFIG-based wind power generation," *IEEE Transactions on Power Systems*, vol. 28, no. 2, pp: 1373–1384, 2013.

On Optimizing the Aerodynamic Load Acting On the Turbine Shaft of PMSG-Based Direct-Drive Wind Energy Conversion System

***Abstract*—The blade's rotational sampling to the spatial distributed wind velocities will induce 3P oscillating aerodynamic torque during the wind energy generation process. This causes the turbine drive-train bare high aerodynamic load because the generator is driven by this aerodynamic torque through it. Moreover, the system's inherent resonant mode will also be induced by the aerodynamic load, causing fatal damage to the whole system. To damp the serious aerodynamic load of the PMSG-based direct-drive wind energy conversation system (WECS), a new power control strategy with damping injection is proposed in this paper. The proposed method is realized by adding a compensation torque, which is proportional to the small-signal value of the generator speed, into the system torque control loop. Both the aerodynamic load and the system's inherent resonant mode could be well damped if the proposed method were adopted. Theoretic analysis is verified by experimental results performed by a 10kW WECS established in the laboratory.**

***Index Terms*—wind power generation; PMSG; aerodynamic load; natural resonant mode suppression; damping injection; power spectrum density**

NOMENCLATURE

v, V_N	Wind velocity and rated wind velocity (m/s)
C_p, C_{pmax}	Power coefficient and its maximum value
C_T, C_{Tmax}	Torque coefficient and its maximum value
λ, λ_{opt}	Tip speed ratio and its optimum value
λ_{max}	Maximum tip speed ratio
k_T	Fit coefficient
J_r	Moment of inertia of the blade (kg·m^2)
J_g	Moment of inertia of the generator (kg·m^2)
K_s	Shaft stiffness (kg/s^2)
B_s	Friction coefficient (kgm/s)
R	Radius of the turbine (m)
ρ	Air density (kg/m^3)
ω_r, ω_g	Rotor speed and generator speed (rad/s)
ω_{ref}	Generator speed reference signal (rad/s)
ω_{rN}, ω_{gN}	Rated rotor and generator speed (rad/s)
ω_{com}	Compensation generator speed (rad/s)
θ_s	Shaft electrical angle (rad)
T_r, T_g	Aerodynamic and generator torque (N·m)
T_g^*	Generator torque reference (N·m)
T_s	Shaft torque (N·m)
$T_{g,comp}$	Compensation torque (N·m)
k_g	Torque amplification gain
V_{dc}, V_l	DC-link and DC-bus voltage (V)
i_{dc}	DC-link current (A)
ω_n	Natural resonant frequency (rad/s)
ξ	System inherent damping factor (kgm/s)
k_{comp}	Compensation gain
P_r	Aerodynamic power (W)
P_{dc}	Generated power of the WECS (W)
P_{rN}, P_{dcN}	Rated aerodynamic and electrical power (W)

I. INTRODUCTION

The development in the use of renewable energy is becoming the key solution to the serious energy crisis and environmental pollution now. Among various kinds of renewable energy, wind energy is by far the fastest growing energy for its free availability, environmental friendliness, policies fostering, and the maturity of turbine techniques; and, it has become a research focus and priority all over the world [1]-[3].

Nowadays, the most commonly used variable-speed turbine structures are doubly fed induction generator (DFIG) based wind energy conversion system (WECS) and direct-drive permanent-magnet synchronous generator (PMSG) based WECS [4]-[5]. To the DFIG, the presence of a gearbox that couples the wind turbine to the generator causes problems. The gearbox suffers from faults and requires regular maintenance. The reliability of the variable-speed wind turbines can be improved significantly by using the PMSG, because of which it has received much attention in wind energy application now. In addition, the PMSG based WECS also has the property of simple structure, high power factor and high efficiency. Therefore, the system structure under consideration in this paper is chosen as the direct-drive PMSG-based WECS.

The main components of a direct-drive PMSG based WECS include a turbine rotor, a drive-train, a PMSG, a full rated power electronic conversion system, and a transformer for grid connection. The system energy generation process can be typically synthesized as: the wind turbine captures the power from wind by means of turbine blades and converts it to mechanical power. The PMSG is driven by the rotating turbine through the drive-train and converts the energy from mechanical to electrical. After adjusting by the power electronics system, the generated power is then injected into the utility grid [6]-[7]. During this process, because the wind speed distribution is far from being uniform throughout the area swept by the blades of a wind turbine (the swept area is very large), wind speeds measured at different points of the swept area may substantially differ, both in its mean and turbulent components, known as wind shear effect [6]. In addition, to a horizontal wind turbine, the airflow in front of the tower is forced to bypass it, making the airflow take a lateral speed whereas its axial speed de-

creases, and this is called tower shadow effect [6]. The wind shear and tower shadow effects will induce 3nP (n=1, 2, 3…) (mainly 3P) oscillating component in the captured aerodynamic torque and further make the drive-train bear high torque ripple, defined as aerodynamic load in this paper, because the 3P oscillating torque is propagating down the system through it. The direct impacts brought by the aerodynamic load are: on the one hand, the drive-train is more likely to be fatigue breakdown, thus to shorten the useful life of the WECS; on the other hand, the system's inherent resonant mode will be easily excited because the drive-train shaft of the multi-pole PMSG-based WECS is rather "soft" and prone to oscillation according to references [8]. This oscillation will lead to the fluctuation in the output power with a frequency usually being as low as 0.1–10Hz which tends to coincide with the frequencies associated with power system interarea oscillations (0.1–2.5 Hz) [9]. As a result, instability issues are expected for the power system with high wind-power penetrations if no aerodynamic load mitigation technique is adopted for the PMSG-based WECS.

In order to damp the aerodynamic load, suppress the oscillations and avoid instability, the most commonly used method is to add external damping to the WECS. A popular way is to mount the damping rubber on the drive-train shaft. However, it is costly and needs additional installation space on the drive-train shaft. Another choice, which can be seen in [10], is to apply damping by means of blade pitching for variable pitch WECS. However, this scheme requires a fast regulation of the blade pitches. The most useful way is to apply active-damping techniques either on the generator-side or on the grid-side [11]–[15]. It is known that the grid-side inverter is usually used to adjust the active and reactive power of the WECS to meet the grid code, there is no more control flexibility to achieve damping injection [12]-[14]. Therefore, active damping from the generator-side becomes a better choice and some researches can be found in the published literatures. In [8], [15], a damping strategy is proposed to control the stator current and the energy stored in the dc-link capacitor. By periodically short-term charging and discharging the dc-link capacitor, energy is stored in the capacitor and the load current varies. This in turn influences the torque in such a way that it counteracts the oscillations and provides effective damping. However, accurate identification of the frequency and phase angle of the generator speed oscillations is needed.

The intended contribution of this paper is to demonstrate that the difficulty in damping the aerodynamic load and suppressing the oscillations can be achieved by using a power control strategy proposed. The rest of this paper is organized as follows: the PMSG-based direct-drive WECS under consideration is modeled as a two-mass model in section II, where the system inherent damping and natural resonant frequency is obtained through modeling analyses. In section III, a novel active-damping injection scheme is proposed to mitigate the aerodynamic load. Since the proposed scheme requires the knowledge of the small signal value of the generator speed, an estimation method based on the power flow analysis is further proposed to obtain this signal. Before conclusions, a fourth part gives out the experimental verifications performed by a 10kW PMSG-based direct-drive variable-speed WECS.

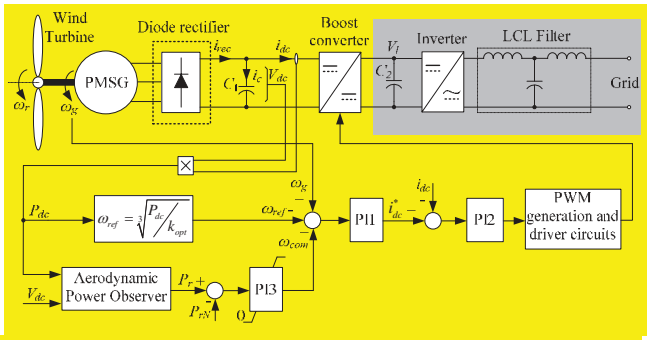

Fig.1 System configuration of the adopted 10kW PMSG-based direct-drive variable-speed WECS

II. System Modeling and Analysis

A. System Structure

The system configuration studied in this paper is depicted in Fig.1. It is constructed by a PMSG-based direct-drive fixed-pitch wind turbine. Through a diode rectifier, the output power of PMSG is transferred to a boost converter which is used to optimally regulate the output power of the turbine. The optimized power is then connected to the grid by the inverter. To balance the generated power and the power injected into the grid, the dc-bus voltage V_l is usually stabilized by the inverter [16]-[17]. Hence, it is reasonable to treat the dc-bus voltage as an ideal voltage source when analyzing the power control strategy of the turbine. Meanwhile, the overall power optimization is achieved by introducing the well known power feedback maximum power point tracking (MPPT) control method into the control system at low wind velocities and the passive soft-stalling control strategy at above rated wind velocities [18]-[19], which is shown in the lower part of Fig.1. In low wind velocity region, the output power of the turbine P_{dc} is firstly sensed and used to calculate the optimum generator speed reference according to the pre-learned aerodynamic characteristics. If the generator speed is controlled to follow this optimum reference very well, the output power can be easily optimized. Whenever the wind velocity exceeds rated value, a generator speed compensation signal ω_{com} generates and is added to the speed control loop, aiming to reduce the generator speed, further to limit the power of the WECS. The operational principle can be referred to [18]. In addition, to make the electrical torque controllable in the adopted system structure, torque control loop is further adopted which is indirectly realized by controlling the dc-link current i_{dc}, as depicted in Fig.1.

B. System Modeling

The well known modeling method for the WECS is using subsystem modeling method. This method first separates the whole system into several interconnected subsystems and then models each subsystem so as to obtain the entire system model. The system shown in Fig.1 can be structured as aerodynamic subsystem, mechanical subsystem and electrical subsystem. The modeling methods for each subsystem are given in the following.

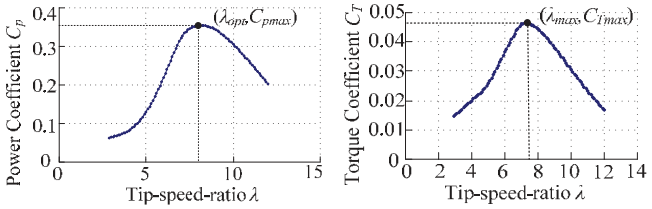

(a) (b)

Fig.2 Power and torque coefficient of the adopted turbine: (a) power coefficient; (b) torque coefficient.

1). *aerodynamic subsystem*

According to the Aerodynamics, the aerodynamic power and torque captured by the turbine blades can be expressed as

$$P_r = \frac{1}{2}\rho\pi R^2 \cdot C_p(\lambda) \cdot v^3 \tag{1}$$

$$T_r = \frac{1}{2}\rho\pi R^3 \cdot C_T(\lambda) \cdot v^2 \tag{2}$$

Since the fixed-pitch wind turbine is adopted in this paper, its power coefficient $C_p(\lambda)$ and torque coefficient $C_T(\lambda)$ (as shown in Fig.2 (a) and (b) respectively) are only varied with tip-speed-ratio λ and they satisfy

$$C_p(\lambda) = \lambda C_T(\lambda) \tag{3}$$

where in (1)-(3), the tip-speed-ratio λ is a parameter defined as

$$\lambda = \frac{\omega_r R}{v} \tag{4}$$

Using polynomial approximation to the C_T-λ curve, we have

$$C_T(\lambda) = C_{T\max} - k_T(\lambda - \lambda_{\max})^2 \tag{5}$$

To the adopted wind turbine, $C_{T\max}$=0.048, $\lambda_{\max}$=7.2, k_T=0.002254. Detailed parameters of the WECS are shown in Table I.

2). *mechanical subsystem*

Conceptually, the mechanical structure can be arranged into several rigid bodies linked by flexible joints. The amount of these joints or degrees of freedom determines the order of the model. Even a few degrees of freedom will give rise to high order nonlinear models. Therefore, it is important to consider in the model just those degrees of freedom that are directly coupled to the control. According to [20], although simple models may not characterize thoroughly the dynamic behavior of the entire WECS, much can be learnt from them. Particularly, simple models are very helpful for analysis on power control strategies and for the controller design, whereas the unmodeled dynamics can be treated as uncertainties. By this reason, the model presented here includes just the torsion mode of the drive-train, as shown in Fig.3, where the drive-train is modeled as two rigid bodies linked by a flexible shaft. Thus, from Fig.3, one can obtain the model of the mechanical subsystem as

$$\begin{bmatrix} \dot{\theta}_s \\ \dot{\omega}_r \\ \dot{\omega}_g \end{bmatrix} = \begin{bmatrix} 0 & 1 & -1 \\ -K_s/J_r & -B_s/J_r & B_s/J_r \\ K_s/J_g & B_s/J_g & -B_s/J_g \end{bmatrix} \cdot \begin{bmatrix} \theta_s \\ \omega_r \\ \omega_g \end{bmatrix} + \begin{bmatrix} 0 & 0 \\ 1/J_r & 0 \\ 0 & -1/J_g \end{bmatrix} \cdot \begin{bmatrix} 0 \\ T_r \\ T_g \end{bmatrix} \tag{6}$$

TABLE I PARAMETERS OF WECS

Parameters of the turbine	Value	Parameters of the PMSG	Value
Radius of the turbine R (m)	3.7	Number of pole-pairs	8
Numbers of blades	3	Moment of inertia of the generator J_g (kg·m^2)	0.32
Moment of inertia of the blade J_r (kg·m^2)	38	Rated output power P_{dcN} (kW)	12
Rated rotor power P_{rN} (kW)	10	Permanent magnet flux ψ (wb)	1.28
rated wind velocity V_N (m/s)	10.5	Rated generator speed ω_{gN} (rad/s)	23
Max power coefficient C_{pmax}	0.35	Winding Resistance R_s (Ω)	1.2
Optimum tip-speed-ratio λ_{opt}	8.2	Winding inductance L (mH)	3.6
Rated rotor speed ω_{rN} (rad/s)	23	Rated output voltage (rectified to DC) V_{dcN} (V)	320
Shaft stiffness K_s (N·m/rad)	620	Friction coefficient B_s (N·m·s/rad)	0.14

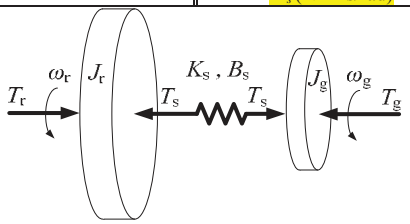

Fig.3 Two-mass model of the drive train

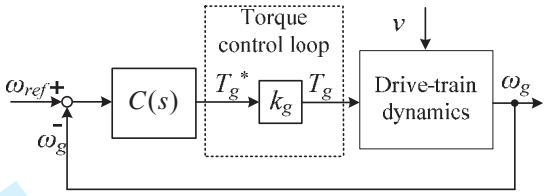

Fig.4 Simplified control block diagram of the WECS

3). *electrical subsystem*

Because the mechanical time constant is much greater than the electrical time constant due to the system's high moment of inertia, it is reasonable to assume the generator torque to track the torque reference without delay. Based on this assumption, we have

$$T_g = k_g T_g^* \tag{7}$$

Normally, the torque dynamics is much faster than the speed dynamics for a generator because of its large inertia. That is equally saying, the dc-link voltage (i.e. the generator rectification voltage) V_{dc} has a much slower dynamics than that of the dc-link current i_{dc}. From this point of view, the system configuration can be simplified to Fig.4, in which $C(s)$ stands for the transfer function of speed regulator PI1 in Fig.1.

4). *entire WECS linear model and analysis*

Using small signal analysis to (2), (5)-(7) at a certain stable operational point $Q(V_Q, \omega_Q)$, the open-loop linear model of the WECS, with the inputs and outputs being $[\tilde{v} \quad \tilde{T}_g^*]^T$ and $[\tilde{T}_s \quad \tilde{\omega}_g]^T$ respectively, can be obtained as

$$\begin{bmatrix} \tilde{T}_s \\ \tilde{\omega}_g \end{bmatrix} = G(s) \begin{bmatrix} \tilde{v} \\ \tilde{T}_g^* \end{bmatrix} = \begin{bmatrix} G_{11}(s) & G_{12}(s) \\ G_{21}(s) & G_{22}(s) \end{bmatrix} \cdot \begin{bmatrix} \tilde{v} \\ \tilde{T}_g^* \end{bmatrix} \tag{8}$$

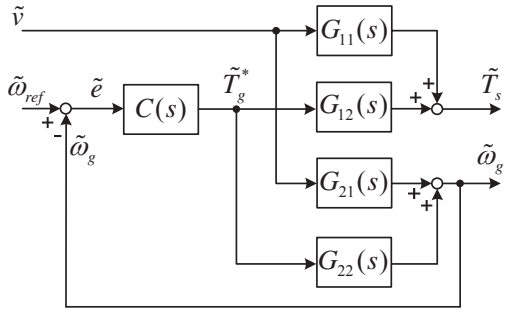

Fig.5 WECS linear model and control

The detailed contents of $G(s)$ in (8) are given on Appendix I.

Hence, Fig.4 can be redrawn as Fig.5, from which the closed-loop transfer function from $[\tilde{v} \quad \tilde{\omega}_{ref}]^T$ to $[\tilde{T}_s \quad \tilde{\omega}_g]^T$ can be obtained as

$$\begin{bmatrix} \tilde{T}_s \\ \tilde{\omega}_g \end{bmatrix} = T(s) \begin{bmatrix} \tilde{v} \\ \tilde{\omega}_{ref} \end{bmatrix} = \begin{bmatrix} T_{11}(s) & T_{12}(s) \\ T_{21}(s) & T_{22}(s) \end{bmatrix} \cdot \begin{bmatrix} \tilde{v} \\ \tilde{\omega}_{ref} \end{bmatrix} \tag{9}$$

The detailed contents of $T(s)$ in (9) are given on Appendix II. Known from the above analysis, due to the spatial distribution of the wind velocity, the effective wind velocity on the rotor plane has a 3P oscillation component. This component will not only induce 3P torque ripple in aerodynamic torque according to (2), but also will make the drive-train bear 3P oscillation torque, defined as aerodynamic load, according to (9). The response of the closed-loop characteristics of aerodynamic load is determined by $T_{11}(s)$ in (9). Moreover, in this equation, $T_{12}(s)$ gives the response of the closed-loop characteristics of shaft torque caused by tracking the optimum generator speed reference, defined as transient load. Because generator speed control is a basic need in realizing power regulation, transient load is inevitable. Moreover, $T_{21}(s)$ and $T_{22}(s)$ determine the closed-loop performance of the generator speed under varying winds and generator speed reference respectively.

To know the response of the shaft torque better, the bode diagrams of the transfer functions $T_{11}(s)$, $T_{12}(s)$, $T_{21}(s)$ and $T_{22}(s)$ at 8m/s wind velocity are plotted in Fig.6. It is noticeable the existence of a poorly damped oscillation mode at about 8Hz. This mode will be excited by the aerodynamic load when the system operational condition changes due to wind or electrical load variations, potentially causing fatigue damage to the drive-train. In addition, speed oscillations will also be induced whenever the oscillation mode is exited, as shown in Fig.6 (d), causing flicker on the electric lines.

The most obvious approach to mitigate the oscillation magnitude of the generator speed is to slow down the response of generator speed, which can be achieved by reducing the gains of speed regulator $C(s)$. Note, however, that transfer function of $T_{11}(s)$ is lower-bounded by (find the expression of $T_{11}(s)$ in Appendix II)

$$|T_{11}(s)| \geq |G_{11}(s)| - |G_{21}(s)| \cdot |T_{12}(s)| \tag{10}$$

Whenever the generator speed response slows down (i.e. gains of $C(s)$ is reduced), $|T_{12}(s)|$ (or the transient load) decreases according to the expression of $T_{12}(s)$ shown in Appendix II. One can then easily conclude from (10) that the aerodynamic load increases. Therefore, the transient load and the aerodynamic load compromise each other. As mentioned in section I, the source of this problem is the lack of damping in the system. Thus, the aerodynamic load and the vibration mode can be attenuated by adding external damping into the system.

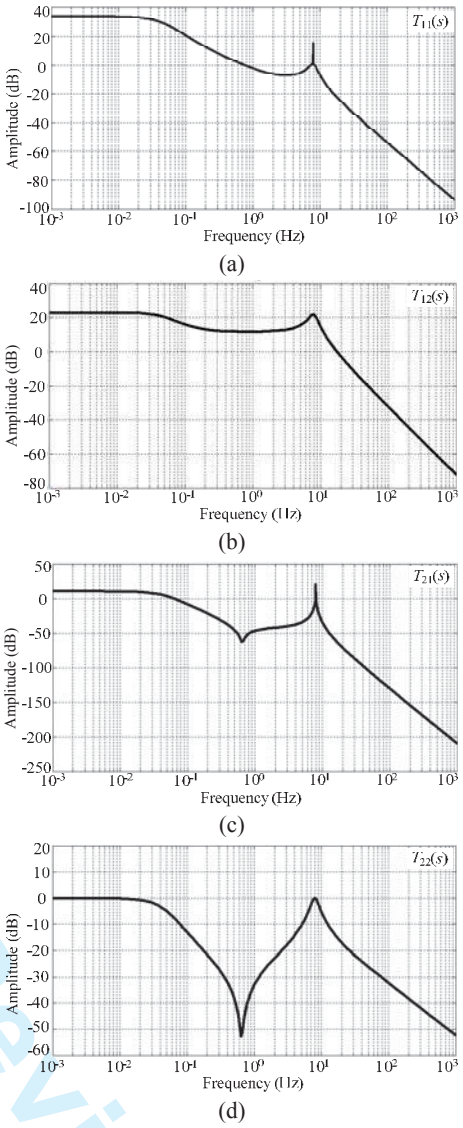

Fig.6 Closed-loop characteristics of the WECS: (a) $T_{11}(s)$; (b) $T_{12}(s)$; (c) $T_{21}(s)$; (d) $T_{22}(s)$.

III. Novel Aerodynamic Load Reduction Method

A. *System inherent damping analysis*

Usually, the wind-turbine inertia is much larger than that of the generator inertia ($J_r >> J_g$), so the dynamics of the rotor speed is much slower than that of the generator speed. Therefore, it is reasonable to assume the rotor speed to be constant compared with the generator speed dynamic. Based on this assumption, one can obtain the small signal model of (6) as

$$\dot{\tilde{\omega}}_r = \tilde{\omega}_g - \frac{K_s}{J_r}\tilde{\theta}_s \tag{11}$$

$$\dot{\tilde{\omega}}_g = \frac{K_s}{J_g}\tilde{\theta}_s - \frac{B_s}{J_g}\tilde{\omega}_g - \frac{1}{J_g}\cdot\frac{\partial T_g}{\partial \omega_g}\tilde{\omega}_g \tag{12}$$

$$\dot{\tilde{\theta}}_s = -\tilde{\omega}_g \tag{13}$$

$$\ddot{\tilde{\theta}}_s = \dot{\tilde{\omega}}_r - \dot{\tilde{\omega}}_g \tag{14}$$

From (11)-(14), the dynamic of the shaft electrical angle can be expressed as a second-order system

$$\ddot{\tilde{\theta}}_s + 2\xi\omega_n\dot{\tilde{\theta}}_s + \omega_n^2\tilde{\theta}_s = 0 \tag{15}$$

where

$$\omega_n = \sqrt{K_s\left(\frac{1}{J_r}+\frac{1}{J_g}\right)} \tag{16}$$

$$\xi = \frac{B_s(J_r+J_g)}{2J_rJ_g\omega_n} + \frac{1}{2J_g\omega_n}\cdot\frac{\partial T_g}{\partial \omega_g} \tag{17}$$

In the above equation, notice that $J_r >> J_g$ and $(\omega_n J_g) >> B_s$, (17) can be simplified as

$$\xi \approx \frac{1}{2J_g\omega_n}\cdot\frac{\partial T_g}{\partial \omega_g} \tag{18}$$

The system's inherent damping is expressed in (18), which indicates that the inherent damping of the WECS is decided by the J_g, ω_n as well as the small-signal ratio of generator electrical torque with respect to generator speed ($\partial T_g/\partial\omega_g$). Because J_g, ω_n are intrinsic parameters of the system, they can't be modified once the system is selected. Alternatively, the only way to increase the system damping is to increase ($\partial T_g/\partial\omega_g$). It can be easily found out that a larger ($\partial T_g/\partial\omega_g$) results in a stronger damping effect. As a result, a compensation torque $T_{g,comp}$, which is proportional to the small signal value of the generator speed can be added in the generator torque loop to damp the aerodynamic load, as shown in Fig.7.

B. System analysis after damping injection

According to the above analysis, the compensation torque should be proportional to the small signal value of the generator speed, that is

$$T_{g,comp} = k_{comp}\tilde{\omega}_g \tag{19}$$

From Fig.7, we have

$$T_g = k_g T_g^* + k_{comp}\tilde{\omega}_g \tag{20}$$

Using small signal analysis to (2), (6) and (20) at the steady state $Q(V_Q, \omega_Q)$, the open-loop transfer function shown in (8) can be renewed as (21) after damping injection.

$$\begin{bmatrix}\tilde{T}_s\\ \tilde{\omega}_g\end{bmatrix} = G_d(s)\begin{bmatrix}\tilde{v}\\ \tilde{T}_g^*\end{bmatrix} = \begin{bmatrix}G_{11d}(s) & G_{12d}(s)\\ G_{21d}(s) & G_{22d}(s)\end{bmatrix}\cdot\begin{bmatrix}\tilde{v}\\ \tilde{T}_g^*\end{bmatrix} \tag{21}$$

where the expressions of $G_d(s)$ are shown on Appendix III.

Then, the system closed-loop transfer function can be obtained as

$$\begin{bmatrix}\tilde{T}_s\\ \tilde{\omega}_g\end{bmatrix} = T_d(s)\begin{bmatrix}\tilde{v}\\ \tilde{\omega}_{ref}\end{bmatrix} = \begin{bmatrix}T_{11d}(s) & T_{12d}(s)\\ T_{21d}(s) & T_{22d}(s)\end{bmatrix}\cdot\begin{bmatrix}\tilde{v}\\ \tilde{\omega}_{ref}\end{bmatrix} \tag{22}$$

where in (22), the transfer function $T_d(s)$ has similar expressions to $T(s)$, as shown on Appendix II. Notice should be taken that the expressions of $G(s)$ should be replaced with $G_d(s)$.

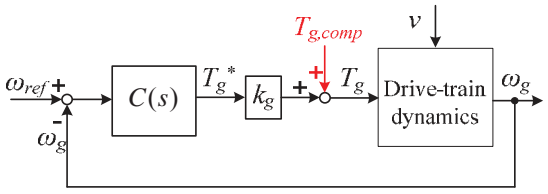

Fig.7 Control with damping injection

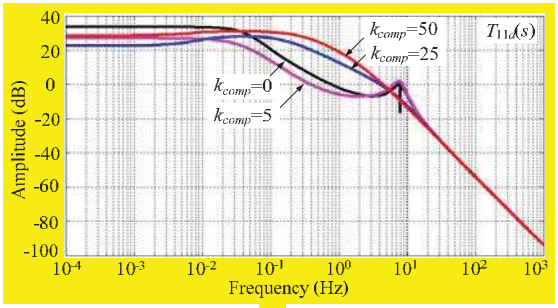

(a)

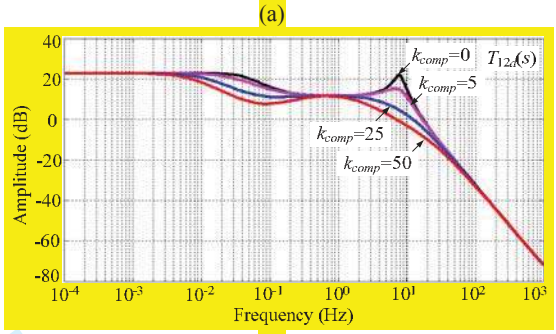

(b)

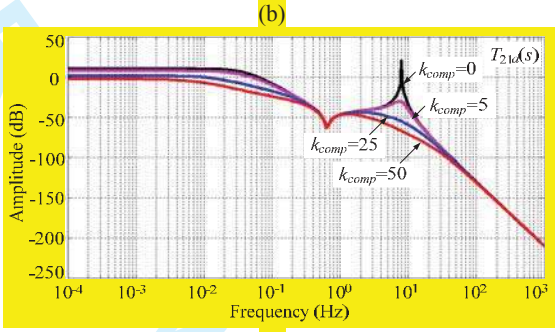

(c)

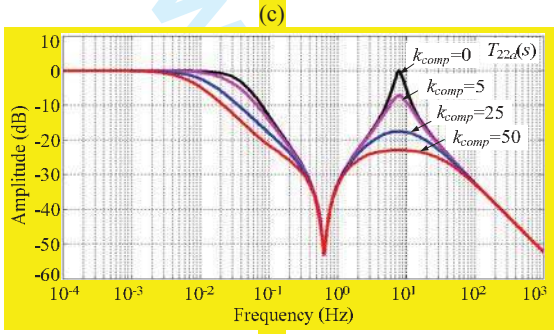

(d)

Fig.8 Closed-loop characteristics of the WECS: (a) $T_{11d}(s)$; (b) $T_{12d}(s)$; (c) $T_{21d}(s)$; (d) $T_{22d}(s)$.

With the proposed active-damping scheme, the bode diagrams of the closed-loop transfer functions of the aerodynamic load and generator speed, known as $T_{11d}(s)$, $T_{12d}(s)$, $T_{21d}(s)$ and

$T_{22d}(s)$, with different k_{comp} are plotted in Fig.8 under wind velocity 8m/s. One can see that not only the aerodynamic load has gotten a reduction without increasing the transient load, but also the system vibration mode can be dramatically reduced with the active damping scheme. The damping effect is stronger with a larger compensation gain. However, on the one hand, a new vibration mode at a lower frequency generates with larger compensation gains, as can be seen in Fig.8 (a), and the aerodynamic load ultimately increases; on the other hand, the frequency response of the generator speed changes with the compensator, and again, a larger compensation gain has a stronger effect. Hence, the choice of the compensation gain should consider the tradeoff between the damping effect and the system response. Finally, the compensation strength is optimally chosen as k_{comp}=10 in this paper.

C. *Way to obtain the small signal value of generator speed*

Known from the above analysis, the system can be well damped if the compensation torque which is proportional to the small signal value of generator speed had been added in the torque control loop. However, the sensor used to detect the generator speed is usually an incremental encoder which continuously outputs the rotor position information. Therefore, it is difficult to get the small-signal value of the generator speed in the real application due to noise issues. Moreover, the rotor position cannot even be obtained in some speed sensorless WECS. In this case, other strategies should be considered for the identification of the small signal value of generator speed.

This paper declares that the generator speed information can be obtained from the electrical power flow, which provides the basis for the compensator implementation.

To the WECS studied in this paper, the power flow in the dc link can be expressed as follows:

$$V_{dc} i_{dc} = T_g \omega_g - P_{dc} \tag{23}$$

Again, notice the fact that the torque dynamics is much faster than the speed dynamics for a generator because of its large inertia. Ignoring the torque dynamics, (23) can be rewritten as

$$T_{gQ} \tilde{\omega}_g = V_{dc} i_{dc} - (T_{gQ} \omega_Q - P_{dc}) \tag{24}$$

In the power balanced control, the steady power flow ($T_{gQ}\omega_Q$ -P_{dc}) is equal to zero. Thus, (24) can be simplified as

$$\tilde{\omega}_g = \frac{V_{dc}}{T_{gQ}} \cdot i_{dc} \tag{25}$$

From (25), one can conclude that the small signal of generator speed is proportional to the dc-link capacitor current. That is to say, the small signal value of generator speed can be indirectly obtained through detecting the dc-link capacitor current. Then, combine (19) and (25), the damping injection method can be achieved.

IV. Experimental Verification

In order to verify the theoretical analyses, experimental results are given in this section. The experiments are done based on a 10kW PMSG-based direct-drive WECS laboratory test-rig setup shown in Fig.9. The experimental test-rig has a structure shown in Fig.1 and its control principle is a combination of

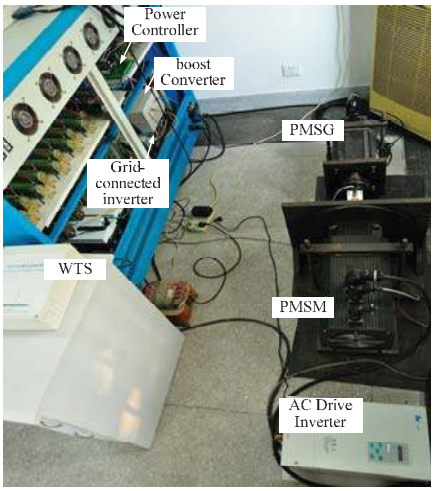

Fig.9 Laboratory test rig

Fig.1 and Fig.7. The system parameters are listed in Table. I. Regulator PI1, PI2 and PI3 are tuned through experiments and their proportional and integral gains are: K_{p1}=0.23, K_{I1}=0.18, K_{p2}=5, K_{I2}=20, K_{p3}=0.1, K_{I3}=2. During experiments, in order to apply different kinds of wind velocities to the WECS, the wind turbine itself is emulated by a permanent magnet synchronous motor (PMSM) driving a PMSG. The parameters of the PMSM working in torque control mode, where the torque demand is given by the wind turbine simulator (WTS) based on a TMS320F2812 digital signal processor (DSP) from Texas Instruments (TI). The same turbine characteristic, as shown in Fig.2, is also programmed in the WTS to perfectly simulate the wind turbine's static and dynamic performance. The correctness of the WTS is verified in the previous work [21]. Particularly, the wind speed model used in chapter 3, reference [22] is adopted here to simulate the wind shear and tower shadow effects.

A. *Operation without damping injection*

In this experiment, the compensation torque is not added to the control loop, i.e. k_{comp}=0. Fig.10 and Fig.11 show the system responses. Fig.10 (a) plots a wind speed signal and its power spectrum density constructed with the adopted wind model. It can be clearly observed that the average wind speed is 7.5m/s and there is an energy concentration at about 8Hz (frequency of 3P for the average rotor speed can be calculated out as ω_r=16.8rad/s because the WECS is working in MPPT mode). When this wind velocity is applied to the WECS, The energy concentration at around 8Hz in the aerodynamic torque can also be observed, as shown in Fig.10 (b). Since this vibration frequency is very close to the system natural resonant frequency determined by (16), the system natural resonant mode has been excited, causing high aerodynamic load and speed oscillations, as can be seen in Fig.10 (c) and (d). It not only makes the drive-train of the WECS more likely to be damaged by the high aerodynamic load, but also deteriorates the power quality and induces flickers on the electric lines.

What's more, it can be further noticed from Fig.11 that the low-frequency component of the dc-link current has the same

frequency, phase angle, and trends with the generator speed, which keeps good pace with the theoretic analyses.

B. *Operation with damping injection*

The system responses with the proposed active-damping scheme under the same conditions are shown in Fig. 12 and 13. Still, because the wind contains high 3P resonant energy, 3P oscillation component in the aerodynamic torque can be found, as shown in Fig.12 (a). However, thanks to the generator torque

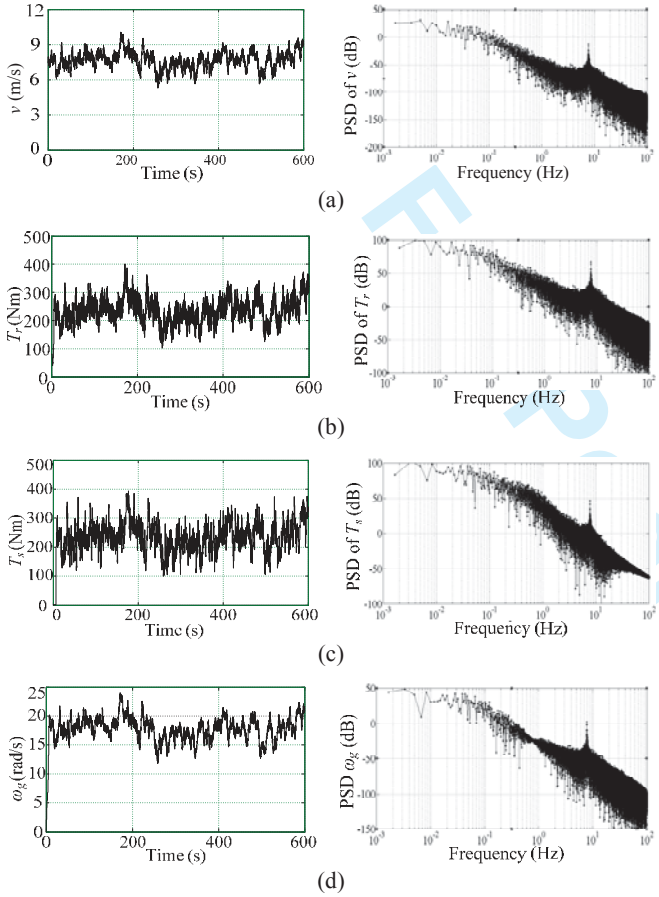

Fig.10 System response without damping injection: (a) wind velocity and its power spectrum density (PSD); (b) aerodynamic load and its PSD; (c) shaft torque and its PSD; (d) generator speed and its PSD.

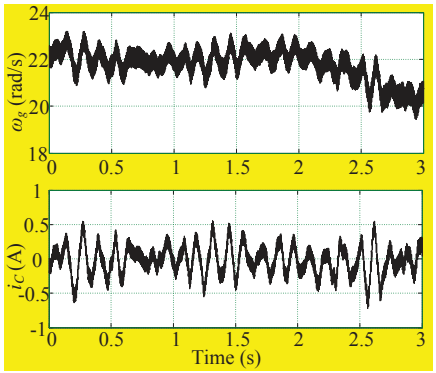

Fig.11 Relationship between the generator speed and capacitor current without damping injection

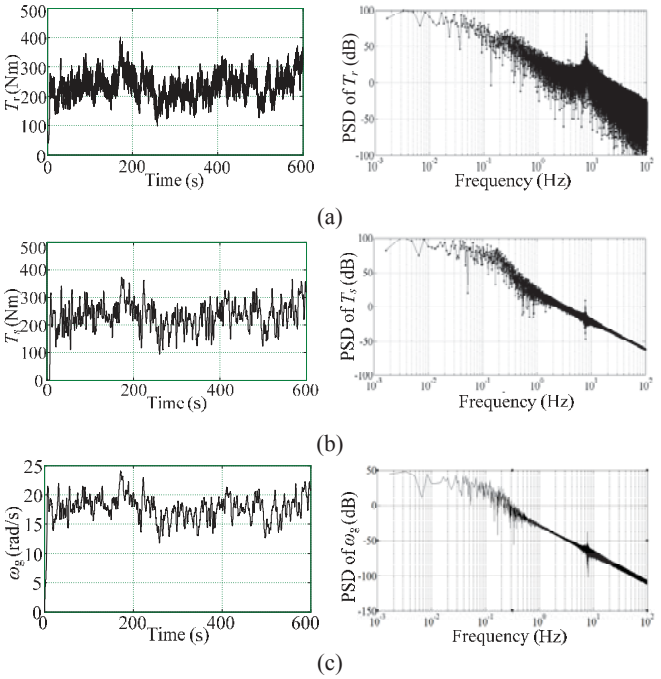

Fig.12 System response with damping injection: (a) aerodynamic load and its PSD; (b) shaft torque and its PSD; (c) generator speed and its PSD.

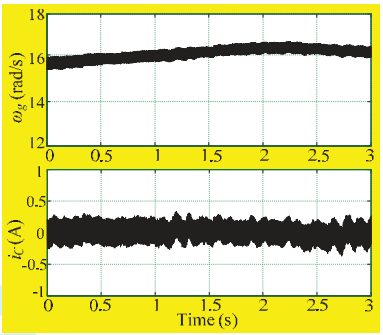

Fig.13 Relationship between the generator speed and capacitor current with damping injection

compensation proposed, the oscillations in the shaft torque and generator speed are both dramatically damped (nearly 50dB), as can be seen in Fig.12 (b) and (c). In addition, the low-frequency oscillations of generator speed and dc-link current can not be observed anymore in Fig.13. All the evidences show that the proposed method can indeed well damp the aerodynamic load and the system resonant mode.

C. *System efficiency analysis with and without damping*

From the above analysis, one can get to know that the proposed damping injection method can help attenuate the serious aerodynamic load. In this section, study is carried out on the system efficiency. The research focus is mainly laid on whether the system efficiency will be affected or not if the damping injection method had been adopted.

The power variations with respect to the wind velocity before and after adopting the damping injection method are plotted in Fig.14. And the variations of power coefficients on these two conditions are plotted in Fig.15. From Fig.15, it can be observed that though higher power coefficient falling

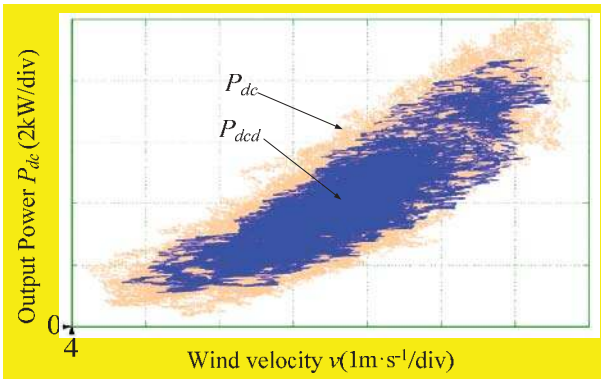

Fig.14 Output power of the WECS versus wind velocity. P_{dc} stands for the output power without damping and P_{dcd} strands for that with damping.

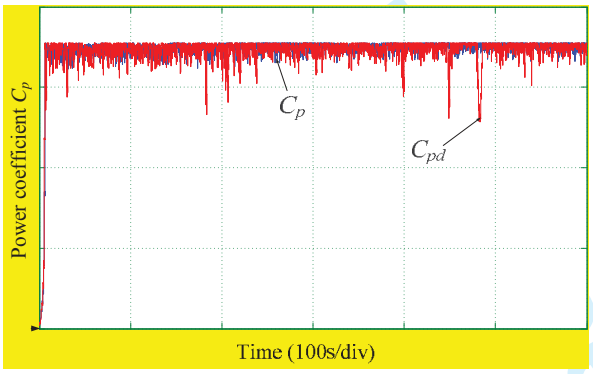

Fig.15 Power coefficient curve. C_p stands for the power coefficient without damping and C_{pd} strands for that with damping.

appears after using the proposed damping injection method, it is not much. From Fig.14, one can see that the power variations on both conditions follow the same pattern and are very close to each other. This evidence shows that the proposed method has little impact on the system overall efficiency. Besides, a decreasing in power variations can be observed in Fig.15. This indicates that the proposed method also features smaller power oscillations.

V. Conclusion

This paper mainly focuses on proposing a power control strategy to damp the serious aerodynamic load acting on the turbine shaft of PMSG-based direct-drive WECS. Through modeling analysis, the system's inherent damping factor is firstly found out. The result shows that the inherent damping for this kind of WECS structure is very small and the system resonant mode is prone to be excited by the aerodynamic load. It is also found out that the oscillation information is contained in the dc-link capacitor current. Thus, the dc-link capacitor current is detected and applied to the compensation strategy which can provide positive damping to the system.

Appendix I
Expressions of $G(s)$ in (8)

$$G_{11}(s)=\frac{J_g\cdot k_r(v_Q,\omega_Q)}{B_r(v_Q,\omega_Q)}\cdot\frac{s(1-\frac{s}{z_0})}{d(s)} \tag{A1}$$

$$G_{12}(s)=-k_g\cdot\frac{(1-\frac{s}{z_0})(1-\frac{s}{z_1})}{d(s)} \tag{A2}$$

$$G_{21}(s)=\frac{k_r(v_Q,\omega_Q)}{B_r(v_Q,\omega_Q)}\cdot\frac{(1-\frac{s}{z_0})}{d(s)} \tag{A3}$$

$$G_{22}(s)=\frac{k_g}{B_r(v_Q,\omega_Q)}\cdot\frac{1+b_{q1}s+b_{q2}s^2}{d(s)} \tag{A4}$$

where in (A1)-(A4)

$$b_{q1}=\frac{B_s+B_r(v_Q,\omega_Q)}{K_s} \tag{A5}$$

$$b_{q2}=\frac{J_r}{K_s} \tag{A6}$$

$$z_0=-\frac{K_s}{B_s} \tag{A7}$$

$$z_1=-\frac{B_r(v_Q,\omega_Q)}{J_r} \tag{A8}$$

$$B_r(V_Q,\omega_Q)=\rho\pi R^4k_T\left[R\cdot\omega_Q-\lambda_{\max}\cdot V_Q\right] \tag{A9}$$

$$k_r(V_Q,\omega_Q)=\rho\pi R^4k_T\left[R\cdot\omega_Q-(1-\frac{C_{T\max}}{k_T\lambda_{\max}^2})\lambda_{\max}\cdot V_Q\right] \tag{A10}$$

and the $d(s)$ is

$$d(s)=1+a_1s+a_2s^2+a_3s^3 \tag{A11}$$

Where in (A11), a_1, a_2 a_3 are determined by

$$a_1=\frac{K_sJ_r+K_sJ_g+B_sB_r(v_Q,\omega_Q)}{K_sB_r(v_Q,\omega_Q)} \tag{A12}$$

$$a_2=\frac{B_sJ_r+B_sJ_g+J_gB_r(v_Q,\omega_Q)}{K_sB_r(v_Q,\omega_Q)} \tag{A13}$$

$$a_3=\frac{J_rJ_g}{K_sB_r(v_Q,\omega_Q)} \tag{A14}$$

Appendix II
Expressions of $T(s)$ in (9)

$$T_{11}(s)=G_{11}(s)-\frac{G_{21}(s)G_{12}(s)C(s)}{1+G_{22}(s)C(s)} \tag{A15}$$

$$T_{12}(s)=\frac{G_{12}(s)C(s)}{1+G_{22}(s)C(s)} \tag{A16}$$

$$T_{21}(s)=\frac{G_{21}(s)}{1+G_{22}(s)C(s)} \tag{A17}$$

$$T_{22}(s)=\frac{G_{22}(s)C(s)}{1+G_{22}(s)C(s)} \tag{A18}$$

where regulator C(s) is chosen as

$$C(s)=\frac{0.23s+0.18}{s} \tag{A19}$$

APPENDIX III
EXPRESSIONS OF $G_d(s)$ IN (21)

$$G_{11d}(s)=\frac{k_r(v_Q,\omega_Q)\cdot k_{comp}}{\left[B_r(v_Q,\omega_Q)+k_{comp}\right]}\cdot\frac{(1-\frac{s}{z_0})(1-\frac{s}{z_2})}{d_1(s)} \quad \text{(A20)}$$

$$G_{12d}(s)=\frac{k_g\cdot B_r(v_Q,\omega_Q)}{\left[B_r(v_Q,\omega_Q)+k_{comp}\right]}\cdot\frac{(1-\frac{s}{z_0})(1-\frac{s}{z_1})}{d_1(s)} \quad \text{(A21)}$$

$$G_{21d}(s)=\frac{k_r(v_Q,\omega_Q)}{\left[B_r(v_Q,\omega_Q)+k_{comp}\right]}\cdot\frac{(1-\frac{s}{z_0})}{d_1(s)} \quad \text{(A22)}$$

$$G_{22d}(s)=\frac{k_g}{\left[B_r(v_Q,\omega_Q)+k_{comp}\right]}\cdot\frac{1+b_{q1}s+b_{q2}s^2}{d_1(s)} \quad \text{(A23)}$$

where in (A20)-A(23)

$$z_2=-\frac{k_{comp}}{J_g} \quad \text{(A24)}$$

$$d_1(s)=1+a_{1d}s+a_{2d}s^2+a_{3d}s^3 \quad \text{(A25)}$$

and

$$a_{1d}=\frac{K_s(J_r+J_g)+k_{comp}\left[B_s+B_r(v_Q,\omega_Q)\right]+B_sB_r(v_Q,\omega_Q)}{K_s\left[B_r(v_Q,\omega_Q)+k_{comp}\right]} \quad \text{(A26)}$$

$$a_{2d}=\frac{J_r(B_s+k_{comp})+J_gK_s\left[B_r(v_Q,\omega_Q)+B_s\right]}{K_s\left[B_r(v_Q,\omega_Q)+k_{comp}\right]} \quad \text{(A27)}$$

$$a_{3d}=\frac{J_rJ_g}{K_s\left[B_r(v_Q,\omega_Q)+k_{comp}\right]} \quad \text{(A28)}$$

REFERENCES

[1] Xu She, Huang A.Q., Fei Wang, Burgos R., "Wind energy system with integrated functions of active power transfer, reactive power compensation, and voltage conversion," *IEEE Transactions on Industrial Electronics*, vol.60, no.10, pp.4512- 4524, 2013.

[2] Liserre, M., Cárdenas, R., Molinas, M., Rodriguez, J., "Overview of multi-MW wind turbines and wind parks," *IEEE Transactions on Industrial Electronics*, vol.58, pp.1081-1095, 2011.

[3] Barote L., Marinescu C., Cirstea M.N., "Control structure for single-phase stand-alone wind-based energy sources," *IEEE Transactions on Industrial Electronics*, vol.60, no.2, pp: 764-772, 2013.

[4] Thanh Hai Nguyen, Dong-Choon Lee, "Advanced fault ride-through technique for PMSG wind turbine systems using line-side converter as STACOM," IEEE Transactions on Industrial Electronics, vol.60, no.7, pp: 2842~2850, 2013.

[5] Arani M.F.M., EI-Saadany E.F., "Implementing virtual inertia in DFIG-based wind power generation," *IEEE Transactions on Power Systems*, vol. 28, no. 2, pp: 1373–1384, 2013.

[6] Fernando D. Bianchi, Hernan De Battista, Ricardo J. Mantz, "Wind turbine control systems principles, modeling and gain scheduling design," *Springer-Advances in Industrial Control Series*, 2006.

[7] Dale S. L. Dolan, Peter W. Lehn, "Simulation model of wind turbine 3p torque oscillations due to wind shear and tower shadow," *IEEE Transactions on Energy Conversion*, vol. 21, No.3, pp: 717-724, 2006.

[8] A. Hansen, G. Michalke, P. Sørensen, T. Lund, and F. Iov, "Coordinated voltage control of DFIG wind turbines in uninterrupted operation during grid faults," *Wind Energy*, vol. 10, No. 1, pp: 51–68, 2007.

[9] S. Brownlees, B. Fox, D. Flynn, and T. Littler, "Wind farm induced oscillations," in *Proc. 41st Int. UPEC*, vol. 1, pp: 118–122, 2006.

[10] S. Jockel, B. Hagenkort, T. Hartkopf, and H. Schneider, "Direct-drive synchronous generator system for offshore wind farms with active drive train damping by blade pitching," in *Proc. EWEC*, 2001, pp: 991–994.

[11] M. Bierhoff and F. Fuchs, "Active damping for three-phase PWM rectifiers with high-order line-side filters," *IEEE Transactions on Industrial Electronics*, vol. 56, no. 2, pp: 371–379, 2009.

[12] M. S. El-Moursi, B. Bak-Jensen, and M. H. Abdel-Rahman, "Novel STATCOM controller for mitigating SSR and damping power system oscillations in a series compensated wind parks," *IEEE Trans. Power Electron.*, vol. 25, no. 2, pp: 429–441, 2010.

[13] R. Varma, S. Auddy, and Y. Semsedini, "Mitigation of subsynchronous resonance in a series-compensated wind farm using FACTS controllers," *IEEE Trans. Power Del.*, vol. 23, no. 3, pp: 1645–1654, 2008.

[14] B. Rigby, N. Chonco, and R. Harley, "Analysis of a power oscillation damping scheme using a voltage-source inverter," *IEEE Transactions on Industrial Applications.*, vol. 38, no. 4, pp: 1105–1113, 2002.

[15] Geng Hua, Xu Dewei, Wu Bin and Yang Geng, "Active damping for tortional vibrations in PMSG based WECS," *in 5th IEEE Applied Power Electronics Conference and Exposition*, pp: 2126–2131, 2010.

[16] Ranjan Vepa, "Nonlinear, optimal control of a wind turbine generator," *IEEE Transactions on Energy Conversion*, vol.26, No.2, pp: 468-478, 2010.

[17] I. Serban, C. Marinescu, "A sensorless control method for variable-speed small wind turbines," *Renewable Energy*, vol.43, pp: 256-266, 2010.

[18] Jiawei Chen, Jie Chen, Chunying Gong, "New overall power control strategy for variable-speed fixed-pitch wind turbines within the whole wind velocity range," *IEEE Transactions on Industrial Electronics*, vol.60, no.7, pp: 2652-2660, 2013.

[19] Haque M.E., Negnevitsky M., and Muttaqi K.M., "A novel control strategy for a variable-speed wind turbine with a permanent-magnet synchronous generator," *IEEE Transaction on Industrial Applications*, vol.46, pp.331-339, 2010.

[20] S. Muyeen, M. Ali, R. Takahashi, T. Murata, J. Tamura, Y. Tomaki, A. Sakahara, and E. Sasano, "Comparative study on transient stability analysis of wind turbine generator system using different drive train models," *IET Renewable Power Generation*, vol. 1, pp: 131–141, 2007.

[21] Jiawei Chen, Jie Chen, Chunying Gong, "Design and analysis of dynamic wind turbine simulator for wind energy conversion system," *in 38th Annual Conference on IEEE industrial Electronics Society*, Montreal, Canada, 2012, pp: 971-977.

[22] Pedro Rosas, "Dynamic influences of wind power on the power system. Kongens Lyngby," Ph. D. Dissertation, Denmark, Technical University of Demark, 2003.